NAVAL POSTGRADUATE SCHOOL
Monterey, California

THESIS

A MODEL FOR DEFORMATION OF CONTINUOUS FIBER COMPOSITES UNDER ISOTHERMAL CREEP AND THERMAL CYCLING CONDITIONS.

by

Myles Esmele II

December 1997

Thesis Advisor: Indranath Dutta

Approved for public release; distribution is unlimited.

REPORT DOCUMENTATION PAGE

Form Approved OMB No. 0704-0188

1. AGENCY USE ONLY *(Leave blank)*	2. REPORT DATE December 1997	3. REPORT TYPE AND DATES COVERED Master's Thesis

4. TITLE AND SUBTITLE A Model For Deformation Of Continuous Fiber Composites under Isothermal Creep and Thermal Cycling Conditions.	5. FUNDING NUMBERS
6. AUTHOR(S) Myles Esmele II	
7. PERFORMING ORGANIZATION NAME(S) AND ADDRESS(ES) Naval Postgraduate School Monterey CA 93943-5000	8. PERFORMING ORGANIZATION REPORT NUMBER
9. SPONSORING/MONITORING AGENCY NAME(S) AND ADDRESS(ES)	10. SPONSORING/MONITORING AGENCY REPORT NUMBER

11. SUPPLEMENTARY NOTES The views expressed in this thesis are those of the author and do not reflect the official policy or position of the Department of Defense or the U.S. Government.

12a. DISTRIBUTION/AVAILABILITY STATEMENT Approved for public release; distribution is unlimited.	12b. DISTRIBUTION CODE

13. ABSTRACT *(maximum 200 words)*

A one-dimensional analytical model for axial deformation of continuous fiber reinforced metal-matrix composites under both thermal cycling and isothermal creep, with or without externally applied stresses, has been developed. Fibers in the model are considered to be non-creeping, thermo-elastic solids, whereas the matrix is considered to be thermo-elasto-plastic and creeping. The model accounts for the strain history of the composite, and allows for changing matrix creep mechanisms via the use of unified creep laws. The use of unified creep laws allows separation of the overall instantaneous creep strain rate into dislocation creep and diffusional creep components, which can be further separated into power law breakdown, pipe diffusion controlled power law, volume diffusion controlled power law, Coble and Nabarro-Herring creep. Additionally, the model allows for the incorporation of time-dependent interfacial sliding near the extremities of the fiber due to the existence of interfacial shear stresses. Based on a recent study, interfacial creep has been represented as being controlled by diffusional flow with a threshold stress (Bingham flow). The interfacial creep law allows simulation of non-isostrain deformation across the interface, and thus the model is capable of explaining experimental observations of strain incompatibility across the interface near fiber-ends. It is envisioned that such a model will be useful in discerning the predominant matrix creep mechanism at a variety of time periods for a given applied stress and temperature, and thus make it possible for the generation of transient deformation mechanism maps for composites.

14. SUBJECT TERMS Continuous Fiber, Metal Matrix Composites, Creep Mechanisms, Isostrain, Non-isostrain Deformation Damage, Interfacial Sliding, Deformation Mechanism Maps			15. NUMBER OF PAGES 101
			16. PRICE CODE
17. SECURITY CLASSIFICATION OF REPORT Unclassified	18. SECURITY CLASSIFICATION OF THIS PAGE Unclassified	19. SECURITY CLASSIFICATION OF ABSTRACT Unclassified	20. LIMITATION OF ABSTRACT UL

A MODEL FOR DEFORMATION OF CONTINUOUS FIBER COMPOSITES UNDER ISOTHERMAL CREEP AND THERMAL CYCLING CONDITIONS.

Myles Esmele II
Lieutenant Commander, United States Navy
B.S. Liberal Arts, University of the State of New York, Albany, 1980

Submitted in partial fulfillment of the
requirements for the degree of

MASTER OF SCIENCE IN MECHANICAL ENGINEERING

from the

NAVAL POSTGRADUATE SCHOOL
December, 1997

Author: _____
Myles Esmele II

Approved by: _____
Indranath Dutta, Thesis Advisor

_____
Terry R. McNelley, Chairman
Department of Mechanical Engineering

ABSTRACT

A one-dimensional analytical model for axial deformation of continuous fiber reinforced metal-matrix composites under both thermal cycling and isothermal creep, with or without externally applied stresses, has been developed. Fibers in the model are considered to be non-creeping, thermo-elastic solids, whereas the matrix is considered to be thermo-elasto-plastic and creeping. The model accounts for the strain history of the composite, and allows for changing matrix creep mechanisms via the use of unified creep laws. The use of unified creep laws allows separation of the overall instantaneous creep strain rate into dislocation creep and diffusional creep components, which can be further separated into power law breakdown, pipe diffusion controlled power law, volume diffusion controlled power law, Coble and Nabarro-Herring creep. Additionally, the model allows for the incorporation of time-dependent interfacial sliding near the extremities of the fiber due to the existence of interfacial shear stresses. Based on a recent study, interfacial creep has been represented as being controlled by diffusional flow with a threshold stress (Bingham flow). The interfacial creep law allows simulation of non-isostrain deformation across the interface, and thus the model is capable of explaining experimental observations of strain incompatibility across the interface near fiber-ends. It is envisioned that such a model will be useful in discerning the predominant matrix creep mechanism at a variety of time periods for a given applied stress and temperature, and thus make it possible for the generation of transient deformation mechanism maps for composites.

vi

TABLE OF CONTENTS

ACKNOWLEDGMENT

I would like to express my sincere gratitude and appreciation to Professor Indranath Dutta for his advice, support, patience and motivation throughout the thesis process. I am also indebted to Dr. Rajagopalan Nagarajan, Dr. Richard Hashimoto, for the contribution of their time and many useful insights, and before I forget, Lieutenant Commander Jeffery Radwick for helping me unlock the secrets of MATLAB™.

I am highly indebted to Elizabeth and Jerry Innocencio who filled in as my surrogate family during my stay in Monterey, California, while my genuine family resided in Chula Vista, California.

I also would like to thank my spouse, Evelyn, and daughters Junelyn, Lesly, Mylessa, and especially my son, Myles III, for all the love and patience shown over the past years while I was absorbed in graduate study.

x

I.   INTRODUCTION

The evolution of many composite materials is a relatively recent technology compared to metals, polymers and ceramics [Ref. 1]. Fiber composites are hybrid materials in which the internal architecture and composition are varied to produce a "designer material", which is suitable for a specific structural or non-structural application. Some of the advantages of composites over monolithic materials include: (1) increased stiffness, (2) increased strength, (3) lower density, (4) increased fracture toughness, (5) potentially higher fracture toughness, (6) higher temperature capabilities, including greater creep resistance, and (7) tailorable thermal properties, i.e. coefficient of thermal resistance (CTE) and thermal conductivity. In particular, continuously reinforced composites offer substantial improvements in properties over monolithic material for loading along the fiber axis, albeit at the expense of isotropy.

Composites are generally classified into three categories, polymer-matrix composites (PMC), ceramic-matrix composites (CMC), and metal-matrix composites (MMC) [Ref. 2]. PMCs are fairly common, inexpensive, have relatively low strength, and are used in the lower range of the temperature scale (typically less than 500 K, although some PMCs may be used up to 600 K). The fiber reinforcement in PMCs imparts stiffness and strength. Metal-matrix composites (including intermetallic-matrix composites) offer significantly higher temperature capabilities (800 to 1300 K).

Because of the attractiveness of the properties of MMCs over non-reinforced metals, MMCs have found several uses in the aerospace and automotive industries over

the last decade. For instance, the Toyota Motor Company has used metal-matrix composites in diesel engine pistons [Ref. 3], Honda has developed and tested entire Aluminum based MMC engine blocks [Ref. 4], Pratt and Whitney have recently started utilizing aluminum based MMCs for aircraft engine applications, whereas the United States Air Force are using discontinuously reinforced Aluminum composites for various material substitution applications in aging aircraft. Other areas like electronic packaging, where the tailorable coefficient of thermal expansion and thermal conductivity of MMCs offer substantial advantages, have also seen significant growth of MMC applications, e.g., in module frames and card cages.

Many of the applications of MMCs are exposed to high homologous temperatures (T/T_m), either under monotonic or cyclic thermal loading conditions, necessitating the development of detailed fundamental scientific understanding and predictive capabilities to describe the time dependent deformation behavior of the composite as a whole. Typically, reinforcement with fibers enhances the longitudinal creep resistance substantially, whereas transverse creep resistance is relatively unaffected. With all the possible reinforcement geometries, the introduction of ceramic or refractory metal long based fibers offers the most significant improvement in creep characteristics.

Because of this, an understanding of the elevated temperature deformation is crucial to the effective engineering design and development of continuous fiber metal-matrix composites (CFCs) components for engineering applications. Several studies of thermal cycling and creep of MMCs have been reported [Refs. 5-22]. A majority of models of creep/thermal cycling of composites assume that only one matrix deformation

2

mechanism to be operative throughout the creep life of the composite. Further, no model is available that explicitly accounts for the time dependent relaxation mechanisms at the interface. These can result in significant errors in the prediction of the overall composite strain response during creep or thermal cycling.

This thesis proposes an analytical model for longitudinal creep/thermal cycling of continuous fiber reinforced MMCs, incorporating: (1) a unified matrix creep law which is capable of handling changing creep mechanisms as a function of the changing stress state in the matrix, (2) contribution of internal thermal residual stresses to matrix creep, and (3) time-dependent interfacial deformation during creep/thermal cycling prior to fiber breakage. It is envisioned that, in addition to yielding predictive capability and a mechanistic understanding of longitudinal creep of continuous fiber reinforced composites, this model will facilitate the generation of transient deformation maps [Ref. 23] for continuous fiber reinforced composites in the future.

II. BACKGROUND

A. CREEP

Early creep experiments conducted by (1) Jech and Weber [Ref. 24] on titanium and titanium alloys with continuous and discontinuous molybdenum fibers, (2) Dean [Ref. 25] on various nickel based alloys reinforced by continuos 0.25 mm diameter fibers, and (3) Ellison and Harris [Ref. 26] carried out on Inconel 600 with 27 percent volume of continuous and discontinuous tungsten fibers have all demonstrated an increase in the stress rupture life of the composite relative to the appropriate unreinforced matrix alloy. Since the aforementioned composite systems showed some mutual solubility between the fiber and the matrix, the demonstrated increase in the stress rupture life of the composite may have been influenced by the chemical changes in the composite. Creep in silver-tungsten composites containing discontinuous fibers with little or no mutual solubility were investigated by Kelly and Tyson [Ref. 5] also showed similar results. Their investigation indicated that the incorporation of discontinuous fibers greatly reduced the rate of creep of the matrix. In addition, they mention that the rate of creep appears to be governed by the rate of creep in shear at the fiber-matrix interface, which is subject to a high shear stress. De Silva [Ref. 6] did not agree with the mechanism proposed by Kelly and Tyson [Ref. 5], which ignored the matrix tensile stress for both load and creep considerations. The matrix tensile stress cannot be ignored since even small tensile stresses in the matrix produce creep rates comparable to that of the composite. Secondly, the shear-based mechanism did not explain creep in continuous fiber reinforced composites (CFCs). De Silva explained that composite creep is governed by (1) the

5

progressively decreasing matrix shear stress adjacent to the interface in discontinuously reinforced composites, and (2) progressively decreasing matrix normal stress resulting from continued load transfer from the matrix to the fiber in a continuously reinforced composite. Doruk and Yue [Ref. 7] suggested that a closed form equation can be extracted from De Silva's [Ref. 6] studies for the time-dependent increase in creep strain using three assumptions for the formulation of the model: (1) load transfer from matrix to the fiber occurs due to tensile stress relaxation in the matrix until the stresses in the matrix and the fibers reach their steady state values; (2) the distribution of the composite stress between the matrix and the fiber at any instant of the loading is governed by the rule of mixtures,

$$\sigma_c = \sigma_f V_f + \sigma_m V_m$$

(where σ and V are the stress and volume fraction, and the subscripts $c, f,$ and m refer to the composite, fiber and matrix respectively) and, (3) the condition of isostrain elongations is valid during creep. Doruk and Yue's [Ref. 7] for matrix strain ($\Delta\varepsilon_m = \Delta\sigma_m/E$) takes the following form:

$$\frac{\Delta\sigma_m}{E_m} = -\left[1 - \left(1 - V_f\right)\frac{E_m}{E_c^*}\right](\dot{\varepsilon}_s)_m\left[1 + (\beta - 1)\exp\left(-K(\dot{\varepsilon}_s)_m t\right)\right]\Delta t$$

where $t = \sum_{1}^{N}\Delta t$ and $(\dot{\varepsilon}_s)_m$ is a known function of σ_m, and where β is the ratio of the initial creep rate, $\dot{\varepsilon}_i$ to the steady state creep rate, $\dot{\varepsilon}_s$. This theoretical model of the primary creep in a fiber reinforced MMC assumes complete load transfer across the fiber-matrix interface. The creep strain-time relationship in terms of the creep properties of the

6

matrix and the fiber can then be computed. This theoretical model like many others that follow assume isostrain conditions across the fiber-matrix interface, and give reasonable agreement with experimental results.

It is believed that during creep, the matrix undergoes stress relaxation by transferring stress to the fiber [Refs. 6-11]. During a constant stress creep test, one of following may occur: (1) if the applied stress is low, all the of applied stress is eventually supported by the fiber (typically stronger and stiffer than the matrix) following complete matrix stress relaxation, and the composite creep rate becomes zero, or (2) if the applied stress is sufficiently high, following complete stress transfer to the fiber, the fracture strength of the fiber may be reached, causing the fiber to rupture. The stress that distinguishes situation (1) from (2) has been referred to as a threshold stress [Refs. 8,9], below which no permanent microstructual damage occurs. McLean [Ref. 8] showed that below this threshold stress, a composite deforms predominantly by primary creep and above this threshold stress, the composite deforms by primary, a brief secondary, and tertiary creep. The tertiary stage is usually associated with permanent microstructual damage, e.g., fiber fracture [Refs. 8,9]. McLean further concluded that the indirect strengthening by particles or fibers can arise not only by the introduction of a threshold stress for deformation but by altering the deformation kinetics as in the case of nickel-based superalloys, and can be influenced by the dislocation structure.

Matsuura et al. [Ref. 9] carried out creep tests on aluminum composite reinforced with continuous alumina fibers at temperatures of 573 to 773 K to examine the mechanism of high temperature deformation and fracture of the composite in low and high stress

7

ranges (i.e., below and above the threshold stress respectively). These specimens were allowed to creep for a period of time, were subsequently unloaded while still at the creep temperature. It was observed that following unloading, the composite underwent time-dependent strain recovery, with the total composite strain finally settling down to either a finite value, corresponding to the permanent microstructual strain/damage, or to a zero value, suggesting no permanent damage. It was further observed that when the post-recovery strain was non-zero, there was evidence of fiber fracture, unless when the post-recovery strain settled at a zero value, no fiber fracture occurred. It was thus concluded that the threshold stress corresponded to the critical stress reached to initiate fiber fracture, and therefore above this threshold, the composite creep rate would not go to zero. In addition to fiber fracture, it is possible that permanent microstructural damage may also occur by relaxation of interfacial shear stresses by time-dependent interfacial sliding, although no direct evidence of this is available to date.

Bullock et al. [Ref. 10] assumed isostrain conditions across the composite in investigations of creep in Ni-Ni$_3$Al-Cr$_3$C$_2$ composites at 825°C and 980°C as a function of microstructure and fiber aspect ratio, and utilized a separate interfacial boundary layer in their model. By assigning a unique stress dependence (i.e., $\sigma_b = \sigma_{o_b} \left(\dfrac{\dot{\varepsilon}}{\dot{\varepsilon}_{o_b}} \right)^b$ of the power-law, where σ_b is the mean stress of the boundary layer, $\dot{\varepsilon}$ is the strain rate, and σ_{o_b}, ε_{o_b}, and b are constants) to the interfacial boundary layer, they were able to account for the interface deformation. The same power-law relationship is used describe the stress in the

8

matrix and the stress in the fiber ($\sigma_m = \sigma_{o_m}\left(\dfrac{\dot{\varepsilon}}{\dot{\varepsilon}_{o_m}}\right)^m$ and $\sigma_f = \sigma_{o_f}\left(\dfrac{\dot{\varepsilon}}{\dot{\varepsilon}_{o_f}}\right)^f$ respectively,

where σ_m, σ_f are the stresses carried by the fiber and matrix respectively and σ_{o_m}, σ_{o_f},

ε_{o_m}, ε_{o_f}, m and f are constants). With these relationships and the rule of mixture for this

model ($V_f + V_m + V_b = 1$, where V is the volume fraction and the subscripts f, m, and b

refer to the fiber, matrix and boundary respectively), they investigated two cases, (1)

where the stress exponents $f = m = b$, and (2) where the stress exponents are not equal, f

$\neq m \neq b$. However, of these models the analytical results were compared with only a

limited amount of experimental results, since at the time, few experimental studies were

available.

Goto and McLean [Ref. 11] also assume isostrain conditions across the fiber-

matrix interface, and considered a model consisting of a power-law creeping matrix,

reinforced by elastically deforming fibers, and that included the effect of an interfacial

region with different deformation characteristics from those of the fiber and the matrix.

The basic assumption in this model is that the fiber-matrix interface region constitutes a

separate phase of thickness, δ, which is small compared to the fiber radius. This model

addressed two types of interfaces where; (1) fiber-matrix slippage since the thin layer

surrounding the fiber is less capable of supporting a shear stress relative to the matrix

(equivalent to the case where creep strength of the boundary zone is much less than that of

the matrix, i.e., $\dot{\varepsilon}_i \gg \dot{\varepsilon}_m$ for the same applied stress), and (2) matrix strengthening, occurs

since the boundary zone creep strength is greater than that of the matrix, (i.e., $\dot{\varepsilon}_i \ll \dot{\varepsilon}_m$),

9

resulting in local work hardening. In the fiber-slippage model, they assume the case of totally incoherent fiber matrix interfaces the Orowan loops may collapse completely into the boundary and provide a potent mechanism for the transfer of stress between the fiber and the matrix. They add, that the absorption of the dislocation loops into the boundary contributes to boundary slippage. In the case of the work hardened model, they assume an E_m and E_f dependency (Young's Modulus for the matrix and fiber). When $E_m > E_f$, and the dislocations are attracted to the boundary where they will introduce an element of slippage while retaining the overall coherency. They correspond to the ideal strength of the composite. When $E_m < E_f$, the Orowan loops are repelled and stand off at an equilibrium distance from the boundary, where a work hardened zone is zone is created and is unlikely to contribute to boundary slippage.

Dlouhy, Eggeler and Merk [Refs. 12-13] recently studied and modeled the uniaxial creep behavior of short fiber reinforced aluminum alloys. The particular mechanical features that their model explained are: (1) the sharp decrease in the creep rate during the primary stage, (2) the extended secondary creep stage with creep strain modulated by fine oscillations, and (3) the slow increase in strain rate during tertiary creep. They concluded that three elementary processes control creep of short fiber reinforced MMCs: (1) loading of fibers by dislocations, (2) recovery processes in the work hardened zones around the fibers, and (3) multiple breakage of fibers during creep. Their most important result of the study is that primary and tertiary processes are not independent, i.e., stress transfer from the matrix to the fiber is generally thought of as the dominant mechanism during

10

primary creep; however, stresses can be redirected from the fiber back to the matrix when fiber breakage occurs.

Most of the studies [Refs. 7-13] have evolved different forms of the power-law creep equations to represent matrix creep reported in the literature. Doruk and Yue [Ref. 7] used the power creep law for steady-state creep rate:

$$\dot{\varepsilon}_s = A\sigma^n \exp(-\Delta H_c / RT)$$

(where A is a material constant, σ is the stress, n is the stress component, ΔH_C is the creep activation energy, R is the gas constant, and T is the absolute temperature), and attributed the Al/Al$_3$Ni matrix composite to undergo dislocation climb primary creep around $0.5T_m$ assuming a complete load transfer across the fiber-matrix interface. McLean et al. [Refs. 8, 10] also considered that the matrix obeyed the steady state power law represented by $\dot{\varepsilon} = A\sigma^n \exp(-Q/RT)$, or a modified form:

$$\dot{\varepsilon} = A'(\sigma - \sigma_o)^{n'} \exp(-Q'/RT)$$

where σ_o is the threshold or friction stress associated with the reinforcement particles that resist deformation. Bullock, McLean and Miles [Ref. 11] also uses a power-law creep relation (described earlier) for both fiber and matrix:

$$\sigma_f = \sigma_{o_f}\left(\frac{\dot{\varepsilon}}{\dot{\varepsilon}_{o_f}}\right)^f \qquad \sigma_m = \sigma_{o_m}\left(\frac{\dot{\varepsilon}}{\dot{\varepsilon}_{o_m}}\right)^m$$

for γNi-Ni$_3$Al(γ')-Cr$_3$C$_2$ composites under a wide range of shear consideration. Most of the reported literature assumes that only one matrix creep mechanism predominates during the entire creep life of a composite.

11

However, the creep mechanism is not only a function of temperature, but also a function of stress. As discussed previously, the matrix is in a state of continuous stress revision. Therefor, different deformation mechanisms may dominate at different times during a creep test, even at a constant temperature. This is illustrated in Figure 1, which represents a deformation mechanism map [Refs. 23, 27] for pure aluminum with a grain size of 10.0 μm. Assuming that the normalized matrix stress, σ_m/μ (where μ is the shear modulus) is initially in the plastic region in the vicinity of 10^{-2} σ_s/μ, at a homologous temperature, 0.7, the matrix stress is seen to transverse through the Power Breakdown region Law region, the Power Law into the Diffusional Flow.
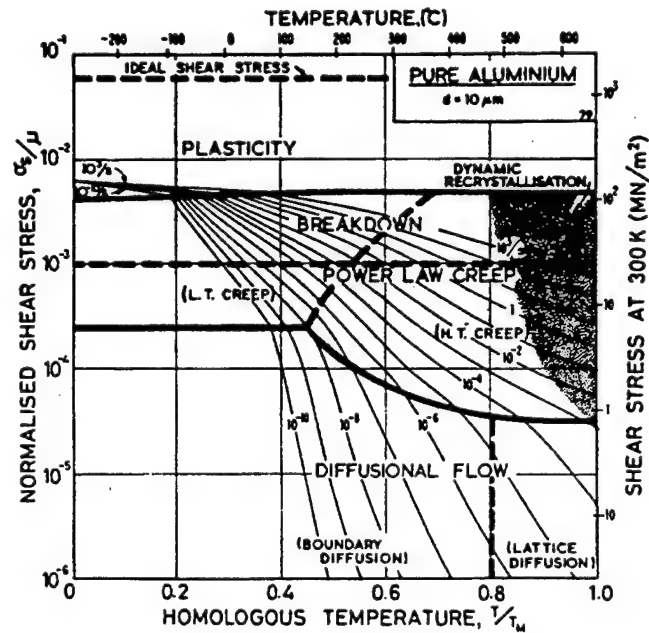
Figure 1. Pure aluminum of grain size 10 μm.

Therefore, in the illustrated example, representing the matrix creep rate by just a power law relationship is not realistic throughout the creep life of the composite. Power law creep represents only a small stress-temperature range for composites as demonstrated above.

Thus, it seems apparent that any composite creep model that is confined to one or two of the matrix creep mechanisms depicted in the deformation mechanisms maps is unlikely to describe the complete creep response over a wide range of applied stresses and temperatures. This necessitates the consideration of a unified matrix creep law for use in composite creep models. Further, the majority of the models represented in the literature [Refs. 7-15], assume that the interface is rigid, i.e., isostrain conditions prevail between the fiber and the matrix.

Significant experimental evidence now exists suggesting that the rigid interface condition between the fiber and the matrix is not always maintained during creep and/or thermal cycling [Refs. 9, 16, 28-35]. Matsuura et al. [Ref. 9] conducted creep test on continuous alumina fiber reinforced aluminum composite. In the case for low stress levels without excessive fiber breakage, and following the primary stage creep, it was determined that the specimens were actually undergoing a measurable finite creep rate on the order of 10^{-9} to 10^{-10} s^{-1}. Weber et al. [Ref. 33] set up experiments to determine the effects of fiber and interface variables on the longitudinal creep of γ-TiAl reinforced with continuous alumina fibers for both weak and strong interfaces at 982°C. A transient creep response was noted in both cases (weak and strong interfaces). Schwenker and Eylon [Ref. 34] conducted similar tests for Ti-6Al-4V composite reinforced with SCS-6 SiC continuous

fibers at low stresses at temperatures of 450, 538 and 650°C. At the two lower temperatures, 450 and 538°C, the predicted creep response was noted; however, at the same low stresses but at a higher temperature of 650°C , a measurable steady state creep rate was observed. Acoustical readings taken during the testing at 650°C at low stresses revealed negligible fiber breakage. At low stress levels, in the absence of fiber fracture, any measurable time-dependent deformation in a continuous reinforced fiber composite may be fully explained by the effect of interfacial creep.

Several other studies involving both creep and thermal cycling have all indicated characteristics best explained by interface creep mechanisms [Refs. 16, 28, 30-32, 35]. Thermal cycling experiments conducted by Dutta et al. [Ref. 16] and Yoda et al. [Ref. 28] demonstrate that the isostrain condition between the fiber and the matrix is not always maintained. Uniaxial longitudinal tensile creep test conducted on continuous reinforced fiber MMCs have been observed to have the matrix extrude beyond the fiber extremities in the absence of fiber breakage. This clearly suggests the breakdown of the isostrain condition, at least near the region of high shear stresses at the fiber ends.

Other studies [Refs. 30-32] also suggest the existence of some form of time-dependent interfacial sliding mechanism. Rosler et al. [Ref. 30] analyzed the effect of diffusional relaxation on creep strength in composite materials, and developed a constitutive equation for the overall creep rate that was dependent on the rate of diffusional flow along the interface. From this creep law, a critical aspect ratio below which creep strength is lost and a critical transition temperature above which creep strength is maintained is eliminated by rapid interface diffusion. According to the model

14

proposed by Kim and McMeeking [Ref. 31] the composite creep strength is equivalently impaired by two independent and separate interface mechanisms: (1) interface with minimal viscous drag (Newtonian viscous slip driven by interfacial shear stress) and (2) rapid diffusion along the interface (diffusional creep driven by the radial stress acting along the interface). Using a similar approach to model the interface deformation with unit cell analysis and a finite element model (FEM), Nimmagadda and Sofronis [Ref. 32] reached similar conclusions but take exception with Kim and McMeeking in the magnitude of the effects of slip and diffusion which underestimates the creep strength of the composite. These two mechanisms, slip and diffusion have the same stress dependence and the same direction of flow; and as such, it may be reasonable to assume that there may be one single interface creep law that combines the effects of both normal and shear stresses at the interface.

Experiments conducted by Funn [Ref. 36] used two models of single fiber composite (SFC) systems in isolation from matrix creep mechanisms. The two systems were chosen such that one had limited mutual solubility between the fiber and the matrix and the other had none in a fiber push-out apparatus to measure the creep characteristics of the interface. The interface was shown to display Bingham flow (diffusional flow with a threshold stress), for both model systems with the range of stresses sustainable by the interface without fiber fracture. An accompanying analytical yielded an explicit constitutive law which describes the stress, temperature, and the matrix and interface property dependence of interfacial creep, and indicated that the experimentally observed

threshold stress is directly attributable to the radial residual stress acting on the fiber matrix interface.

The form of the proposed analytical interfacial creep law is:

$$\dot{\gamma}_I = \frac{4\delta_I d_I \Omega_I}{kTh^3}\left(\tau_i - \tau_o\right)$$

where:

$$\tau_o = 2\left(\frac{\pi h}{\lambda}\right)^3 \sigma_R, \quad \text{is the threshold shear stress,}$$

δ_i - thickness of the grain boundary $\qquad$ Ω_i - atomic volume of the interface,

τ_i - average applied interfacial shear stress $\quad$ Q_i - activation energy for the rate

k - Boltzman constant $\qquad\qquad\qquad\qquad$ controlling process

R - universal gas constant $\qquad\qquad\qquad$ T - absolute temperature

h - peak to peak height of interface $\qquad$ λ - period of the interface

In the present work, this interfacial sliding law is incorporated in the composite creep model, in order to allow for non-isostrain deformation of the fiber and the matrix.

Thermal cycling experiments conducted on continuous fiber reinforced composites offer the most dramatic evidence of an independent interface deformation mechanism and is discussed in detail in the next section.

B.   THERMAL CYCLING

The differences in the coefficient of thermal expansion (CTE) between the matrix and the fiber can induce large internal stresses in the composite during thermal cycling, which can result in the number of unusual effects in the strain response during cycling [Refs. 16-18, 28-32, 37-40].   These effects include: (1) large strain hysteresis, (2) residual plastic strain following one or more thermal cycles, and (3) a highly non-linear thermal expansion coefficient.   These effects have been attributed to: (1) differences in the longitudinal coefficients of thermal expansion between the fiber and the matrix, (2) heating and cooling rates, (3) strain history, and (4) creep deformation.

A number of these thermal cycling experiments conducted on continuous fiber reinforced metal-matrix composites offer the most dramatic evidence of an independent interface deformation mechanism [Refs. 16, 28-32].   These composites usually display a large strain hysteresis during thermal excursions.   A permanent residual strain may also be observed after the first few thermal cycles.   The strain hysteresis usually persists with continued cycling; however, additional residual strains may not necessarily occur. Examples of the strain hysteresis curves are found in (1) Garmong's [Ref. 18] study of Al-Al$_3$Ni eutectic metal-matrix composite cycled between 300 and 850 K, (2) Dries et al. [Ref. 40] rapid thermal cycling of P100 graphite-6061 Al metal-matrix composite cycled between 116 and 394 K, and (3) Mitra et al. [Ref. 17] slow thermal cycling between 298 and 813 K of the same metal-matrix composite as Dries et al. [Ref. 40] studied.   In the above cases, three observations were made, (1) the strain hyteresis was attributed to the varying matrix stress state of the composite, (2) plastic deformation of the matrix at the

lower temperature of the cooling leg contributes to the residual strain, and (3) creep strains at the high temperature end of the thermal cycle. Characteristic curves of strain versus temperature during a thermal cycle may indicate a "knee". The "knee" during the heating leg of the thermal cycle is due to the compressive creep strains induced in the matrix; whereas, during the cooling leg, it is due to the tensile yielding of the matrix.

Dutta et al. [Ref. 16] studied the effects of thermal residual stresses on the strain response of graphite-aluminum continuous fiber composites during thermal cycling which revealed time-dependent strains evident that the matrix has crept out pass the fiber ends to relieve the thermally imposed tensile stress. It was also noted during the experiments, that stress relaxation via matrix creep can give rise to time-dependent strains under isothermal conditions with an external applied stress. After hundreds of cycles in the homologous temperature range between 0.35 and 0.80 of tungsten wire reinforced copper composites by Yoda et al. [Ref. 28], they observed the growth per unit length increased after a given number of cycles with increasing holding time at the upper cycling temperature; and that it was also dependent on fiber length, fiber diameter and fiber volume fraction. Scanning electron micrographs of the 10 volume percent tungsten wire reinforced copper composite in Reference 28 showed the copper matrix extruding pass the ends of the tungsten fibers of 100 µm diameter by as much as 1.0 mm for samples that were initially 10.0 mm long. This observation suggests that interface sliding plays an important role in elevated temperature deformation in this class of material.

A number of analytical representations [Refs. 37-39] modeled the longitudinal strain response of the unidirectionally reinforced composite during thermal cycling.

However, most are based on an one-dimensional isostrain model where the fiber-matrix interface is assumed perfectly bonded, (2) the fiber undergoes thermo-elastic deformation, and (3) the matrix is subject to thermal, elastic, plastic and time dependent strains. Garmong [Ref. 37]makes similar assumptions and assumes that, (1) Poisson effects are dismissed, (2) stresses and strains are uniform within each phase, (3) no interfacial sliding may occur, and (4) the composite is metallurgically stable, i.e., no physical or chemical changes occur in the composite structure during thermal cycling or at exposure elevated temperatures. This was a first step in analyzing composite behavior in conditions of thermal cycling with applied loads helped provided a framework which the various material and test parameters for observations of deformation and failure. Because of these assumptions, the thermal cycling strain response shows a strong dependence on the heating and cooling rate (i.e., slower cooling rates result in greater permanent strains. Another factor is the coefficient of thermal expansion (CTE). The coefficient of thermal expansion modulates non-linearly with temperature due to the varying stress and strain states within the composites during thermal cycling.

Dutta et al. [Ref. 16] used the same assumptions to model the behavior of the strain response of 20 volume percent P100 graphite-6061 Al metal-matrix composite between 300 and 800 K at 1/60 Ks^{-1} during thermal cycling. The results from their analytical work on thermal cycling predicted that, (1) significant creep strains are induced during both legs of the thermal cycle, (2) significant plastic strains are induced in the matrix during cooling, and (3) creep strains result in a strong heating/cooling rate dependence of the strain response.

19

It is not only matrix plastic and creep deformation that may cause progressive degradation of the mechanical properties of the composite [Ref. 17], but damage to the fiber-matrix interface as well. Like the matrix plastic and creep strains, the extent of the interfacial damage depends on the mechanical properties of the fiber and matrix, coefficients of thermal expansion, the heating/cooling rates, as well as the nature of the interface itself. Interfacial damage may occur via interfacial sliding, where the matrix may extrude past the fiber ends or the fiber may extrude pass the matrix. Evidence of interfacial sliding after thermal cycling is found in micrographs of graphite fiber ends extruding pass the aluminum matrix in Reference 17 (slow heating and cooling), and tungsten extruded with respect to the copper matrix in Reference 28 (rapid heating and cooling).

Thus the importance of the fiber-matrix interface, where it may slide, cannot be discounted nor neglected. This necessitates incorporation of interfacial sliding in any phenomenologically correct model of creep and/or thermal cycling.

III. OBJECTIVE

The purpose of this work is to develop a unidirectional model capable of simulating the overall axial strain response of a continuous fiber reinforced metal-matrix composite during both isothermal and thermal cycling conditions, with or without an externally applied stress.

The model incorporates the effects of: (1) thermal history of the composite, and the influence of internal residual stress, (2) evolving matrix deformation mechanisms (due to continuous matrix stress state revision) via the use of unified creep laws, and (3) the breakdown of isostrain conditions at the fiber-matrix interface. The model assumes that the fiber is thermo-elastic, the matrix is thermo-elastic-plastic-creeping (with the creep rate being represented by Garofalo's unified dislocation creep law [Ref. 41], and Frost and Ashby's unified diffusion creep law [Ref. 23]), and that the interface may undergo time-dependent diffusional sliding following a Bigham type law, as proposed in Reference 40.

In the subsequent sections, the following longitudinal creep/thermal cycling models for continuous fiber reinforced composites are presented, (1) with isostrain conditions across the fiber-matrix interface (Section A, Chapter IV), the Isostrain Model, and (2) the model with interfacial sliding (Section B, Chapter IV), the Non-isostrain Model.

IV. ANALYTICAL MODELS

A. ISOSTRAIN CONDITION ACROSS THE INTERFACE, UNIFIED MATRIX CREEP LAW

The following analysis of composite creep is based on a model by Garmong [Ref. 37] as modified by Tyson [Ref. 38]. The model by Garmong and Tyson [Refs. 37, 38] assume that, (1) the composite deformation is one-dimensional, (2) the stresses and strains are uniform within each phase, (3) there is no interface sliding, (4) no chemical or physical changes in the structure (metallurgically stable), (5) the temperature is uniform throughout the composite, (6) fiber is thermo-elastic, and the matrix is thermo-elastic, plastic and creeping and follows the power-law for creep. In the following analysis, Garofalo's unified dislocation creep law [Ref. 41] and Ashby and Frost unified diffusion creep law [Ref. 23] are utilized in order to demonstrate High Temperature Power Law Creep (lattice diffusion controlled creep), Low Temperature Power Law Creep (pipe diffusion controlled creep), Power Law Breakdown Creep, Coble Creep, and Nabarro-Herring Creep. The object is to be able to discuss the predominant creep mechanism at any instant during creep or thermal cycling. In addition, the model incorporates the externally applied stresses under a wide array of initial matrix conditions and applied stress ranges.

For a composite having two phases, the rule of mixtures given below applies:

$$\sigma_c = \sigma_f V_f + \sigma_m V_m \tag{1}$$

23

where, σ and V are the stress and volume fraction, and the subscripts $c, f,$ and m refer to the composite, fiber and matrix respectively. To ensure continuity at the fiber-matrix interface (isostrain), the strain continuity equation may be expressed as:

$$\varepsilon_m = \varepsilon_f \qquad (2)$$

where ε is the strain, and the subscripts m and f refer to the matrix and fiber respectively. The strain of either phase is:

$$\varepsilon = \varepsilon^{th} + \varepsilon^{el} + \varepsilon^{pl} + \varepsilon^{cr} \qquad (3)$$

where the superscripts th, el, pl and cr refer to thermal, elastic, plastic (time independent) and creep deformation. For the temperature range of interest, the fiber for most MMC's may be assumed to be elastic (i.e., $\varepsilon_f^{pl} = \varepsilon_f^{cr} = 0$). The thermal strain relation for the fiber and matrix is:

$$\varepsilon_f^{th} = \int_{T_1}^{T_2} \alpha_f dT \qquad (4a)$$

$$\varepsilon_m^{th} = \int_{T_1}^{T_2} \alpha_m dT \qquad (4b)$$

Where α is the coefficient of thermal expansion (CTE), and T_1, T_2, are the initial and final temperatures respectively. The elastic stress strain relation for the fiber and for the matrix constituent is:

$$\varepsilon_f = \frac{\sigma_f}{E_f} \qquad (5a)$$

$$\varepsilon_m = \frac{\sigma_m}{E_m} \qquad (5b)$$

24

where E is Young's Modulus. The plastic strain, as derived from the Ludwik relation is:

$$\varepsilon_m^{pl} = \left[\frac{\left(\sigma_m - \sigma_m^{ys} \right)}{K_1} \right]^{\frac{1}{n}} \tag{6}$$

where σ_m^{ys} is the matrix yield stress, K_1 and n is the work hardening coefficient and work hardening exponent, respectively.

The creep strain, ε_m^{cr} may be obtained as:

$$\varepsilon_m^{cr} = \int_{T_1}^{T_2} \dot{\varepsilon}_m^{cr} dt \tag{7a}$$

for isothermal creep or

$$\varepsilon_m^{cr} = \int_{T_1}^{T_2} \varepsilon_m^{cr} \left(\frac{dT}{dt} \right)^{-1} dT \tag{7b}$$

for thermal cycling creep, where $\left(\dfrac{dT}{dt} \right)^{-1}$ is the reciprocal of the heating/cooling rate.

The creep rate $\dot{\varepsilon}_m^{cr}$, has contributions from both dislocation based and diffusional mechanisms and may be represented as:

$$\dot{\varepsilon}_m^{cr} = \dot{\varepsilon}_m^{diff} + \dot{\varepsilon}_m^{disl} \tag{8}$$

where the superscripts *diff* and *disl* are for the diffusional and dislocation creep (Appendix A describes the conversion of the relevant creep expressions from the shear strain rate-shear stress ($\dot{\gamma} - \tau$) form given by Ashby and Frost [Ref. 23] to normal- strain rate, normal stress form components, respectively. The diffusional creep rate ($\dot{\varepsilon}_m^{diff}$) may be written as:

25

$$\dot{\varepsilon}_m^{diff} = \frac{14\Omega}{kTd^2} D_{eff}^{diff} \sigma_m \qquad (9)$$

where:
$$D_{eff}^{diff} = \left[D_L + \left(\frac{\pi}{d}\right) \delta D_{gb} \right] \qquad (10)$$

$$D_L = D_{o_L} e^{-Q_L/kT} \qquad (11)$$

$$\delta D_{gb} = \delta D_{o_{gb}} e^{-Q_{gb}/kT} \qquad (12)$$

Ω - atomic volume D - diffusivity
d - the matrix grain D_o - frequency factor
δ - effective thickness Q - activation energy for the appropriate
  of the grain boundary   diffusion path
b - Burgers vector k - Boltzman constant
T - absolute temperature

and the subscripts *eff* for effective, L for lattice (volume), *gb* for grain boundary.

The dislocation creep term ($\dot{\varepsilon}_m^{disl}$) may be written in the Sinh form originally

proposed by Garofalo [Ref. 41] as modified by Frost and Ashby [Ref. 23]:

$$\dot{\varepsilon}_m^{disl} = \left(\frac{\sqrt{3}}{\alpha'}\right)^{n1} \frac{AG_m b}{kT} D_{eff}^{disl} \left[\sinh\left(\frac{\alpha'}{\sqrt{3}G_m} \sigma_m\right) \right]^{n1} \qquad (13)$$

where:
$$D_{eff}^{disl} = \left[D_L + \left(\frac{10}{3b^2 G_m^2}\right) \sigma_m^2 a_p D_p \right] \qquad (14)$$

$$a_p D_p = a_p D_{po} e^{-Q_p/kT} \qquad (15)$$

n1 - creep exponent A - creep constant
G_m - shear modulus a - cross sectional area of the dislocation core
     α' - power law breakdown threshold

and the subscript p is for pipe.

Substitution of Equations (9) and (13) into Equation (8), provides the total matrix creep strain:

$$\varepsilon_m^{cr} = \int_{T_1}^{T_2} \left\{ \frac{14\Omega}{kTd^2} D_{eff}^{diff} \sigma_m + \left(\frac{\sqrt{3}}{\alpha'} \right)^{n1} \frac{AG_m b}{kT} D_{eff}^{disl} \left[\sinh\left(\frac{\alpha'}{\sqrt{3}G_m} \sigma_m \right) \right]^{n1} \right\} \left(\frac{dT}{dt} \right)^{-1} dT \qquad (16)$$

The total matrix strain is found by substitution of Equations (4b), (5b), (6) and (16) into the left-hand side of Equation (2) results in;

$$\int_{T_1}^{T_2} \alpha_m dT + \frac{\sigma_m}{E_m} + \left[\frac{\left(\sigma_m - \sigma_m^{ys} \right)}{K_1} \right]^{\frac{1}{n_1}} \pm \int_{T_1}^{T_2} \left\{ \frac{14\Omega}{kTd^2} D_{eff}^{diff} \sigma_m + \left(\frac{\sqrt{3}}{\alpha'} \right)^{n1} \frac{AG_m b}{kT} D_{eff}^{disl} \left[\sinh\left(\frac{\alpha'}{\sqrt{3}G_m} \sigma_m \right) \right]^{n1} \right\} \left(\frac{dT}{dt} \right)^{-1} dT$$

and deriving the fiber strain found by substitution of Equation (4) into the right hand side of Equation (2) after replacing σ_f as a function of σ_m ($\sigma_f = \dfrac{\sigma_a - \sigma_m V_m}{V_f}$), from Equation (1), the rule of mixtures:

$$\int_{T_1}^{T_2} \alpha_m dT + \frac{\sigma_m}{E_m} + \left[\frac{\left(\sigma_m - \sigma_m^{ys} \right)}{K_1} \right]^{\frac{1}{n_1}} \pm \int_{T_1}^{T_2} \left\{ \frac{14\Omega}{kTd^2} D_{eff}^{diff} \sigma_m + \left(\frac{\sqrt{3}}{\alpha'} \right)^{n1} \frac{AG_m b}{kT} D_{eff}^{disl} \left[\sinh\left(\frac{\alpha'}{\sqrt{3}G_m} \sigma_m \right) \right]^{n1} \right\} \left(\frac{dT}{dt} \right)^{-1} dT$$

$$= \int_{T_1}^{T_2} \alpha_f dT + \frac{\sigma_a - \sigma_m V_m}{E} \qquad (17)$$

Following Tyson [Ref. 38] Equation (17) may be expressed in differential (i.e., incremental) form as:

$$\Delta\varepsilon_m = \Delta\varepsilon_f$$
$$\Delta\alpha_m \Delta T + \Delta\varepsilon_m^{el} + \Delta\varepsilon_m^{pl} + \Delta\varepsilon_m^{cr} = \alpha_f \Delta T + \Delta\varepsilon_f^{el} \qquad (18)$$

27

Solving for $\Delta\sigma_m$ after substituting the appropriate expanded terms from Equation (17) into Equation (18), gives the following:

$$\Delta\sigma_m = -\frac{\Delta\alpha\Delta T \pm \left\{ \frac{14\Omega}{kTd^2} D_{eff}^{diff} \sigma_m + \left(\frac{\sqrt{3}}{\alpha'}\right)^{n1} \frac{AG_m b}{kT} D_{eff}^{disl}\left[\sinh\left(\frac{\alpha'}{\sqrt{3}G_m}\sigma_m\right)\right]^{n1}\right\}\left(\frac{\Delta T}{\Delta t}\right)^{-1}\Delta T - \frac{\Delta\sigma_a}{E_f V_f}}{\frac{V_m}{E_f V_f} + \frac{1}{E_m} + \frac{1}{RWH}} \qquad (19)$$

where

$$\Delta\alpha = \alpha_m - \alpha_f \qquad (19a)$$

$$RWH = \frac{d\sigma_m}{d\varepsilon_m^{pl}} = K_1 n\left(\left[\frac{\left(\sigma_m - \sigma_m^{ys}\right)}{K_1}\right]^{\frac{1}{n}}\right)^{n-1} \qquad (19b)$$

In Equation (19), $\Delta\sigma_a = 0$, where $\sigma_a = 0$ or constant for both thermal cycling or isothermal creep/thermal cycling conditions. Therefore, Equation (19) does not account for the effect of an externally applied stress. The methodology of incorporating the effect of σ_a in the solution procedure is outlined later in section IV.A.2.

1. CALCULATION OF INDIVIDUAL MATRIX STRAINS

During each iteration, the incremental strains are calculated as follows:

$$\Delta\varepsilon^{th} = \Delta\alpha\Delta T \qquad (20a)$$

28

$$\Delta \varepsilon_m^{el} = \frac{\Delta \sigma_m}{E_m} \tag{20b}$$

$$\Delta \varepsilon_m^{pl} = \frac{\Delta \sigma_m}{RWH} \tag{20c}$$

$$\Delta \varepsilon_m^{cr} = \int_{T_1}^{T_2} \left\{ \frac{14\Omega}{kTd^2} D_{eff}^{diff} \sigma_m + \left(\frac{\sqrt{3}}{\alpha'} \right)^{n1} \frac{AG_m b}{kT} D_{eff}^{disl} \left[\sinh\left(\frac{\alpha'}{\sqrt{3}G_m} \sigma_m \right) \right]^{n1} \right\} \left(\frac{\Delta T}{\Delta t} \right)^{-1} \Delta T \tag{20d}$$

Finally, the total matrix stress and strain components are updated as:

$$\sigma_{m(i)} = \sigma_{m(i-1)} + \Delta \sigma_m \tag{21a}$$

$$\varepsilon_{(i)}^{th} = \varepsilon_{(i-1)}^{th} + \Delta \varepsilon^{th} \tag{21b}$$

$$\varepsilon_{m(i)}^{el} = \varepsilon_{m(i-1)}^{el} + \Delta \varepsilon_m^{el} \tag{21c}$$

$$\varepsilon_{m(i)}^{pl} = \varepsilon_{m(i-1)}^{pl} + \Delta \varepsilon_m^{pl} \tag{21d}$$

$$\varepsilon_{m(i)}^{cr} = \varepsilon_{m(i-1)}^{cr} + \Delta \varepsilon_m^{cr} \tag{21e}$$

The total matrix creep strain can be further disseminated into Power Law (PL) creep, High Temperature (dislocation lattice diffusion controlled creep) PL creep, Low Temperature (dislocation pipe diffusion controlled creep) PL creep, Power Law Breakdown (PLB) creep, Coble creep, and Nabarro-Herring creep. The following equations were used to determine the individual creep strain components;

Power Law dislocation creep strain:

$$\varepsilon_m^{PL} = \frac{AG_m b}{kT} \left(\frac{\sqrt{3}}{\alpha'} \right)^{n_1} \left[D_L + \frac{10}{3} \left(\frac{\Delta \sigma_{m(i-1)}}{bG_m} \right)^2 a_p D_p \right] \left[\frac{\alpha'}{\sqrt{3}G_m} \Delta \sigma_{m(i-1)} \right]^{n_1} \Delta t \tag{22}$$

29

High Temperature (volume diffusion controlled climb) power law creep strain:

$$\varepsilon_m^{HT\_PL} = \frac{AG_m b}{kT}\left(\frac{\sqrt{3}}{\alpha'}\right)^{n_1}[D_L]\left[\frac{\alpha'}{\sqrt{3}G_m}\Delta\sigma_{m(i-1)}\right]^{n_1}\Delta t \tag{22a}$$

Low Temperature (core diffusion controlled climb) power law creep strain:

$$\varepsilon_m^{LT\_PL} = \frac{AG_m b}{kT}\left(\frac{\sqrt{3}}{\alpha'}\right)^{n_1}\left[\frac{10}{3}\left(\frac{\Delta\sigma_{m(i-1)}}{bG_m}\right)^2 a_p D_p\right]\left[\frac{\alpha'}{\sqrt{3}G_m}\Delta\sigma_{m(i-1)}\right]^{n_1}\Delta t \tag{22b}$$

Power Law breakdown (transition from climb-plus-glide to glide alone) dislocation creep strain:

$$\varepsilon_m^{PLB} = \frac{AG_m b}{kT}\left(\frac{\sqrt{3}}{\alpha'}\right)^{n_1}\left[D_L + \frac{10}{3}\left(\frac{\Delta\sigma_{m(i-1)}}{bG_m}\right)^2 a_p D_p\right]\left[\sinh\left(\frac{\alpha'}{\sqrt{3}G_m}\Delta\sigma_{m(i-1)}\right)\right]^{n_1}\Delta t - \varepsilon_m^{PL}\Delta t$$

$$\tag{23}$$

The Power Law Breakdown creep strain is given in above form when the threshold matrix stress is reached or exceeded (the Power Law for creep strain breaks down).

Coble (grain boundary) diffusional creep strain:

$$\varepsilon_m^{Coble} = \frac{14\Omega}{kTd^2}\left(\frac{\pi}{d}\right)\delta D_{gb}\Delta\sigma_{m(i-1)}\Delta t \tag{24}$$

Nabarro-Herring (lattice) diffusional creep strain:

$$\varepsilon_m^{NH} = \frac{14\Omega}{kTd^2}D_L\Delta\sigma_{m(i-1)}\Delta t \tag{25}$$

where Δt, is the time step in seconds.

Equation (19) is incrementally solved during thermal cycling or isothermal creep (with temperature or time as the independent variable, respectively) using a computer program (Appendix C) written in the **MATLAB**™ programming language.

2.   INCORPORATION OF APPLIED STRESS IN MODEL

The above algorithm does not account for the effect of the applied stress (σ_a), since the term σ_a does not appear in Equation (19) ($\Delta\sigma_a = 0$ for a constant σ_a in both thermal cycling or isothermal creep/thermal cycling conditions).

In order to account for the applied stress (σ_a), one needs to compute the stress induced in the matrix due to σ_a (σ_m^{ap}). Depending on the initial residual matrix stress state (σ_{m_o}) prior to the application of σ_a, six scenarios can occur. They are described in Tables 1 and 2, along with a listing of the corresponding expressions for σ_m^{ap}.

The incorporation of the effect of the applied stress in the initial value of σ_m, prior to the start of the iterative solution outline above, is updated as follows:

$$\sigma_m^{total} = \sigma_{m_o} + \sigma_m^{ap}$$

31

MATRIX LOADING IS IN THE SAME DIRECTION AS THE RESIDUAL MATRIX STRESS.

SCENARIO & CONDITIONS	$\dfrac{\sigma_{mo}}{\sigma_{qp}} \geq 0$	$\Delta\sigma_m^{ap}$ and $\Delta\varepsilon_m^{ap}$
CASE I Matrix is elasto-plastically loaded in the same direction as the residual stress.	$\left|\sigma_{mo}\right| < \left|\sigma_m^{ys}\right|$ and $\left|\sigma_{ap}\right| \geq \left|\dfrac{\sigma_m^{ys} - \sigma_{mo}}{E_m}\right|\left(E_m V_m + E_f V_f\right)$ $\varepsilon_{ps} = \dfrac{\sigma_{ap}}{E_c} - \dfrac{\sigma_m^{ys} - \sigma_{mo}}{E_m} + \dfrac{\sigma_m^{ys}}{E_m}$	$\Delta\sigma_m^{ap} = \left(\sigma_m^{ys} - \sigma_{mo}\right) + K_m\left(\varepsilon_{ps} - \dfrac{\sigma_m^{ys}}{E_m}\right)$ $\Delta\varepsilon_m^{ap} = \varepsilon_{ps} - \dfrac{\sigma_{mo}}{E_m}$
CASE II Matrix is plastically loaded in the same direction as the residual stress.	$\dfrac{\sigma_{mo}}{\sigma_{ap}} \geq 0$ and $\left|\sigma_{mo}\right| \geq \left|\sigma_m^{ys}\right|$ $\varepsilon_{ps} = \dfrac{\sigma_{ap}}{E_c} + \dfrac{\sigma_{mo}}{E_m}$	$\Delta\sigma_m^{ap} = K_m \dfrac{\sigma_{ap}}{E_f V + K_m V_m}$ $\Delta\varepsilon_m^{ap} = \varepsilon_{ps} - \dfrac{\sigma_{mo}}{E_m}$
CASE VI Matrix is elastically loaded in the same direction as the residual stress.	$\left|\sigma_{mo}\right| < \left|\sigma_m^{ys}\right|$ and $\left|\sigma_{ap}\right| < \left|\dfrac{\sigma_m^{ys}}{E_m}\right|\left(E_m V_m + E_f V_f\right)$ $\varepsilon_{ps} = \dfrac{\sigma_{ap}}{E_c} + \dfrac{\sigma_{mo}}{E_m}$	$\Delta\sigma_m^{ap} = \dfrac{\sigma_{ap} E_m}{E_m V_m - E_f V_f}$ $\Delta\varepsilon_m^{ap} = \varepsilon_{ps} - \dfrac{\sigma_{mo}}{E_m}$

TABLE 1. Algorithm to determine σ_m^{total} due to applied stress, σ_a in the same direction as the residual matrix stress.

MATRIX LOADING IS IN THE OPPOSITE DIRECTION THAN THAT OF THE RESIDUAL MATRIX STRESS.

$$\frac{\sigma_{m_o}}{\sigma_{ap}} < 0$$

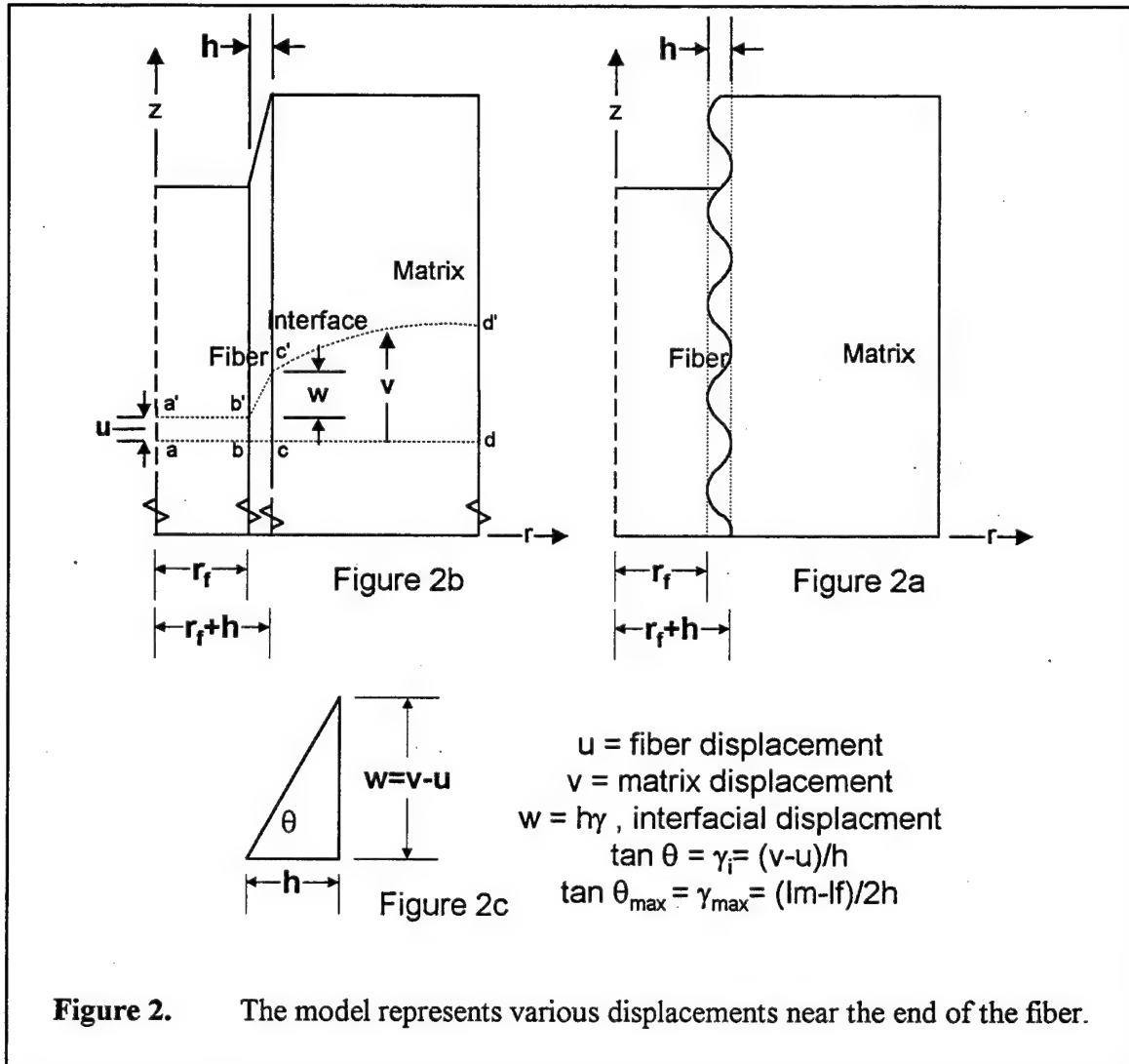| SCENARIO & CONDITIONS		$\Delta\sigma_m^{ap}$ and $\Delta\varepsilon_m^{ap}$
CASE III Matrix is elastically unloaded and elasto-plastically loaded in the opposite direction than that of the residual matrix stress.	$$\left|\sigma_{ap}\right| \geq \frac{\left|\sigma_m^{ys} - \sigma_{mo}\right|}{E_m}\left(E_m V_m + E_f V_f\right)$$ $$\varepsilon_{ps} = \frac{\sigma_{ap}}{E_c} - \frac{\sigma_m^{ys} - \sigma_{mo}}{E_m} + \frac{\sigma_m^{ys}}{E_m}$$	$$\Delta\sigma_m^{ap} = \left(\sigma_m^{ys} - \sigma_{mo}\right) + K_m\left(\varepsilon_{ps} - \frac{\sigma_m^{ys}}{E_m}\right)$$ $$\Delta\varepsilon_m^{ap} = \varepsilon_{ps} - \frac{\sigma_{mo}}{E_m}$$
CASE IV Matrix is elastically unloaded and elastically loaded in the opposite direction than that of the residual matrix stress.	$$\left|\sigma_{ap}\right| < \frac{\left|\sigma_m^{ys}\right|}{E_m}\left(E_m V_m + E_f V_f\right)$$ $$\left|\sigma_{ap}\right| > \frac{\left|\sigma_{mo}\right|}{E_m}\left(E_m V_m + E_f V_f\right)$$ $$\varepsilon_{ps} = \frac{\sigma_{ap}}{E_c} + \frac{\sigma_{mo}}{E_m}$$	$$\Delta\sigma_m^{ap} = \frac{\sigma_{ap}E_m}{E_m V_m - E_f V_f}$$ $$\Delta\varepsilon_m^{ap} = \varepsilon_{ps} - \frac{\sigma_{mo}}{E_m}$$
CASE V Matrix is elastically unloaded only in the opposite direction than that of the residual matrix stress.	$$\left|\sigma_{ap}\right| < \frac{\left|\sigma_m^{ys}\right|}{E_m}\left(E_m V_m + E_f V_f\right)$$ $$\left|\sigma_{ap}\right| \leq \frac{\left|\sigma_{mo}\right|}{E_m}\left(E_m V_m + E_f V_f\right)$$ $$\varepsilon_{ps} = \frac{\sigma_{ap}}{E_c} + \frac{\sigma_{mo}}{E_m}$$	$$\Delta\sigma_m^{ap} = \frac{\sigma_{ap}E_m}{E_m V_m - E_f V_f}$$ $$\Delta\varepsilon_m^{ap} = \varepsilon_{ps} - \frac{\sigma_{mo}}{E_m}$$

TABLE 2. Algorithm to determine σ_m^{total} due to applied stress, σ_a in the opposite direction of the residual matrix stress.

B. NON-ISOSTRAIN UNIFIED LAW ANALYSIS

The conditions across the interface may be modeled as shown in Figure 2. Here, the matrix is allowed to undergo a different longitudinal strain relative to the fiber. This is accommodated by interfacial sliding due to the presence of interfacial shear stresses near the ends of the fiber. The interface may be thought of as a periodic boundary with a

$w = v - u$

u = fiber displacement
v = matrix displacement
w = hγ, interfacial displacment
$\tan \theta = \gamma_i = (v-u)/h$
$\tan \theta_{max} = \gamma_{max} = (l_m - l_f)/2h$

Figure 2c

Figure 2. The model represents various displacements near the end of the fiber.

peak to peak height of length **h**, which is assumed to represent the "width" of the

35

interface, and of periodic lengths, represented by λ. A simplified model based on Figure 2a is shown in Figure 2b. The dotted lines represent the displacements in the fiber, interface and matrix. Dotted line a-d is the initial reference line in the undeformed state. Dotted lines $a'-b'$, $b'-c'$, and $c'-d'$ represent the displacements after longitudinal deformation of the composite has occurred, and u represents the fiber displacement, w is the interfacial displacement(equal to $h\gamma_i$, where γ_i is the interfacial shear strain), and v the matrix displacement. The details of the interfacial geometry are shown in Figure 2c.

On a global scale, it may be assumed that $v \neq f(r)$, i.e., ε_m is constant for all r. However, very close to the interface, $v = f(r)$, and this results in an interfacial shear stress τ_i, which drives interfacial sliding. The interfacial shear strain at any value of z may be represented as:

$$\gamma_i = \frac{v(r = r_f + h) - u(r = r_f)}{h} = \frac{z(1 + \varepsilon_m) - z(1 + \varepsilon_f)}{h}$$

or:
$$\gamma_i = \frac{z}{h}\left(\varepsilon_m - \varepsilon_f\right) \tag{26}$$

where $0 \leq z \leq \frac{l_o}{2}$. At $z = \frac{l_o}{2}$, the shear strain reaches its maximum value, which is given by:

$$\gamma_i^{max} = \frac{l_o}{2h}\left(\varepsilon_m - \varepsilon_f\right) \tag{27}$$

Equation (26) forms the strain continuity equation for the non-isostrain condition, instead of $\varepsilon_f = \varepsilon_m$ for the isostrain condition.

36

In Equation (16), ε_m has four components: ε_m^{th}, ε_m^{el}, ε_m^{pl}, ε_m^{cr}; and ε_f has two

components: ε_f^{th}, ε_f^{el}. These can be found using the same approach as the analysis for

the isostrain condition found in section A of Chapter IV.

The interfacial creep rate proposed in Reference 40 is utilized to find γ_i:

$$\dot{\gamma}_i = K_i\left(\tau_i - \tau_o\right) \tag{28}$$

where:

$$K_i = \frac{4\delta_i D_i \Omega_i}{kTh^3} \tag{28a}$$

The interfacial shear stress τ_i, in Equation (28) may be obtained from the following

relationship (Appendix C):

$$\left(\varepsilon_m - \varepsilon_f\right)\left(z - \frac{l_o - l_c}{2}\right) = (M+N)\tau_i + \frac{Q}{n}\tau_i^n \tag{29}$$

where $M = hK_i\Delta t$

$$N = \left(\frac{1}{G_m} + \frac{1}{K''} + A_{diff}\Delta t\right)r_f \ln\left(\frac{R}{r_f}\right) \qquad A_{diff} = \frac{42\Omega}{kTd^2}\left(D_L + \frac{\pi\delta}{d}D_{gb}\right)$$

$$Q = nr_f^n A_{disl}\Delta t\left(\frac{R^{1-n} - r_f^{1-n}}{1-n}\right) \qquad A_{disl} = \left(\sqrt{3}\right)^{n+1}AD_{eff}\frac{G_m b}{kT}\left(\frac{1}{G_m}\right)^n$$

l_o - Original length of the fiber [m]
l_c - Critical fiber transfer length [m], and may be approximated as:

$$l_c = \frac{\sigma_{f_{cr}}}{2\tau_m^{ys}}d_f$$

$\sigma_{f_{cr}}$ - Fiber fracture stress [Pa]

τ_m^{ys} - Shear yield strength of the matrix [Pa]
d_f - Diameter of the fiber [m]
h - Peak to peak height of interface [m]
Q_i - Activation energy of the appropriate diffusion path [m^{2}s^{-1}]
K - Work hardening coefficient in tension [Pa]
K'' - Work hardening coefficient in shear [Pa] (Appendix D)

G_m - Shear modulus [Pa]
n - Stress exponent
b - Burgers vector [m]
d - Grain size [m]
δ - Effective thickness of the grain boundary [m]
D_{gb} - Grain boundary diffusion [m²s⁻¹]
D_L - Volume diffusion [m²s⁻¹]
D_{eff} - Effective diffusion [m²s⁻¹]
A - Dorn constant (for normal strain rate, $\dot{\varepsilon}$)
Ω - Atomic volume [m³]
k - Boltzmann's constant [1.381e-23 J K⁻¹]
R - Gas constant [8.314 J mole⁻¹ K⁻¹]
T - Absolute temperature [K]
r_f - Radius of the fiber
R - Radius from center of fiber to an arbitrary radial point

The threshold stress (Appendix E), τ_o in Equation (28) may be estimated as:

$$\tau_o = 2\pi^3\left(\frac{h}{\lambda}\right)^3\left[\frac{480}{T} - 0.60\right]\sigma_{R_o} \tag{30}$$

where λ is the period of the interface and σ_{Ro} is the radial residual stress acting on the interface at 300 K.

In incremental form, the interfacial shear strain may be written as:

$$\Delta\gamma_i = \dot{\gamma}_i\Delta t = \frac{4\delta_i D_i \Omega_i}{kTh^3}(\tau_i - \tau_o)\Delta t \tag{31}$$

Equation (26) may be expressed in incremental form as:

$$\Delta\gamma_i = \frac{z}{h}\left(\Delta\varepsilon_m - \Delta\varepsilon_f\right) \tag{32}$$

Substitution of Equation (31) in Equation (32) results in:

$$\left(\Delta\varepsilon_m - \Delta\varepsilon_f\right) = \left(\frac{z}{h}\right)\frac{4\delta_i D_i \Omega_i}{kTh^2}(\tau_i - \tau_o)\Delta t \tag{33}$$

38

Where the terms $\Delta\varepsilon_m$ and $\Delta\varepsilon_f$ are given by Equation (18), Equations (20a) through (20d), Equations (21a) through (21e), and Equations (22) through (25) in section A Chapter IV. Substituting for $\Delta\varepsilon_m$ and $\Delta\varepsilon_f$ in Equation (33), the incremental matrix stress $\Delta\sigma_m$ results in the following equation:

$$\Delta\sigma_m = -\frac{\Delta\alpha\Delta T \pm \left\{\dot{\varepsilon}_m^{cr}\right\}\left(\frac{\Delta T}{\Delta t}\right)^{-1}\Delta T - \frac{\Delta\sigma_a}{E_f V_f} - \left(\frac{z}{h}\right)\frac{4\delta_i D_i \Omega_i}{kTh^2}(\tau_i - \tau_o)\Delta t}{\frac{V_m}{E_f V_f} + \frac{1}{E_m} + \frac{1}{RWH}} \quad (34)$$

where ε_m^{cr} is given by Equation (16).

The procedure to determine the various strains with or without an external applied stress is identical to the isostrain case discussed in Subsections 1 and 2 of Section A Chapter IV.

Sample calculations for the isostrain model are shown in Section A Chapter V.

V. SAMPLE CALCULATIONS

A. MATERIAL PROPERTIES

Results for sample calculations based on the model for isostrain conditions the fiber-matrix interface (Section A Chapter IV) are shown in this chapter. The hypothetical composite consisting of a 0.4 volume fraction of continuous fiber SiC in a 1100 Aluminum matrix. The properties used for the computations are listed below:

	MATRIX (1100 Al)	FIBER (SiC)
Melting Temperature [K]	933.47	
Coefficient of Thermal Expansion (CTE) [1/K]	23e-6	4e-6
Young's Modulus at 300K [Pa]	65000e6	450000e6
Volume Fraction	0.6	0.4
Shear Modulus at 300K [Pa]	25000e6	
Temperature Dependence, $(T_m/G_m)(dG_m/dT)$	-0.5	
Work Hardening Constant [Pa]	500e6	
Work Hardening Exponent	1.0	
Lattice Diffusivity Frequency Factor, D_{lo} [m^2/s]	1.7e-4	
Lattice Diffusion Activation Energy, Q_l [J/mole]	142000	
Grain Boundary pre-exponential, δD_{gbo} [m^3/s]	5e-14	
Grain Boundary Activation Energy, Q_{gb} [J/mole]	84000	
Pipe pre-exponential, $a_p D_{po}$ [m^4/s]	7e-25	
Pipe Activation Energy, Q_p [J/mole]	82000	
Burgers vector, b [m]	2.86e-10	
Atomic Volume, Ω [m^3]	1.66e-29	
Dorn Constant, A $$\dot{\varepsilon} = A\left(\frac{\sigma_m}{G_m}\right)^z \frac{D_{eff} G_m b}{kT}$$	3.4e6	
Stress Exponent for Creep Equation	4.4	
P-L Breakdown Threshold, α' [σ_m/G_m]	1000	
Grain Size, d [m]	25e-6	
Universal Gas constant, R [J/ mole-K]	8.314	
Boltzman constant, k [J/K]	1.38e-23	

TABLE 3.   MATERIAL PROPERTIES and CONSTANTS [Refs. 23, 42, 43]

A non-linear fit was obtained for the yield strength versus temperature data for 1100 Aluminum based on the data taken from reference 43 for temperatures less than or equal to 625 K. A linear fit between the yield strength and temperature greater than 625 K is covered. This is shown in the Figure 3.

Figure 3. Curve fitted yield strength of 1100 aluminum as a function of temperature [Ref. 43].
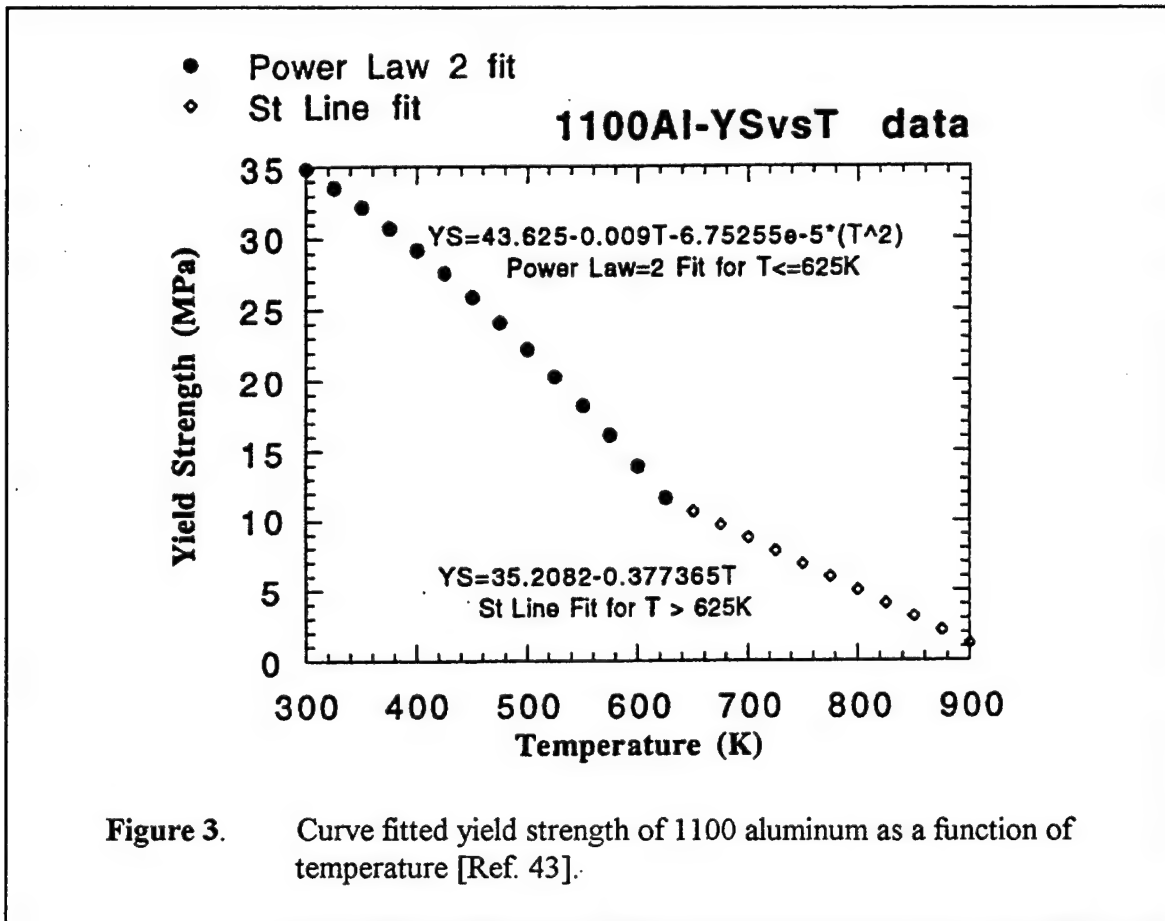
B. THERMAL EXCURSIONS FOR THERMAL CYCLING AND ISOTHERMAL CREEP SIMULATIONS

The Aluminum-SiC composite is cooled from the fabrication temperature (T_{fab}) OF 800 K to ambient temperature of 300 K, at constant rate of 1/60 K/second (Ks^{-1}). At the

fabrication temperature, the matrix stress and strain are assumed to be equal to zero. The final matrix stress and matrix strain following cooling to 300 K are used as inputs for subsequent calculations.

1.   Thermal Cycling Simulation

The composite is heated at a rate of 1.0 Ks^{-1} from 300 to 700 K. The final matrix stress and strain at 700 K are used as inputs for the simulations of the cooling leg from 700 to 300 K at constant rate of 1/60 Ks^{-1}. This heating and cooling half legs constitute one thermal cycle between 300 to 700 K. A discussion of the heating leg of the thermal cycle is presented in Section B.

2.   Isothermal Creep Simulation

Simulations of isothermal creep under conditions of constant applied stresses were conducted at various temperatures (400, 523, 673, and 700 K). The result for isothermal creep at 673 K at an applied stress of 50 MPa are discussed in Section C.

Following the initial conditions from the cooling from fabrication temperature to ambient temperature is heated at 1.0 Ks^{-1} to the creep temperature. Then, the matrix stress and strain states immediately after the application of the external stress are calculated, following which, the time dependent simulation of deformation is carried out.

43

C. THERMAL CYCLING: HEATING LEG FROM 300 TO 700 K

Only a discussion of the heating leg of the thermal when the conditions of zero applied stress is provided to demonstrate the application of the isostrain model to thermal cycling simulations.

The following Figures 4 through 9 represent the various conditions of stresses and strains as the 0.40 volume percent SiC 6061 aluminum metal-matrix composite commencing with an initial residual matrix stress of 36.414 MPa and initial residual strain of -2.1214e-03. (The matrix stress of 36.414 MPa and strain of -2.1214e-03 result from cooling from the fabrication temperature of 800 K to 300K.) The thermal excursion constituted heating from the initial temperature of 300 K to the final temperature of 700 K at a heating rate of 1.0 K per second.

Figure 4 is a plot of the composite strain along the longitudinal direction. Around 390 K, a distinct 'knee' is observed where the composite displays a change in the coefficient of thermal expansion (CTE), which is given by the slope of the strain versus temperature curve.

Figure 5 shows the predicted residual matrix as a function of temperature. As the composite is heated, the matrix stress is progressively relieved. Complete relief of the composite is seen around 360 K where the matrix stress becomes compressive and reaches a maximum (approximately -50 MPa) at around 390 K. At 700 K, a compressive residual matrix stress of 1.9 MPa was predicted. Note that the 'knee' observed in Figure 4 corresponds to the 'knee' in Figure 5.

44

The predicted thermal, elastic, plastic and creeping cumulative strains during the entire heating temperature excursion is depicted in Figure 6. No plastic deformation is observed because the residual stress at all temperatures is less than the temperature dependent matrix yield strength. Around 390 K, matrix creep processes are activated. Because of the presence of compressive matrix stress, compressive creep strains are observed. As expected, the thermal strain monotonically increases with temperature, and elastic strain shows a variation similar to that of the stress. It is evident that the creep deformation after 390 K is responsible for the 'knee' observed in Figure 4.

Figures 7 through 9 shows variation of the incremental creep strain components due to the various mechanisms as function of temperature during heating. The components plotted include both dislocation and diffusional creep. The dislocation creep is further subdivided into power law breakdown creep and total power law, in which total power law can be split up into high temperature power law and low temperature power law creep. These are depicted in Figure 8. The diffusional creep can be further be broken down into Coble and Nabarro-Herring creep, shown in Figure 9.

It is apparent from Figure 7 that the primary contribution to the overall creep strain is from dislocation creep. The total dislocation creep strain may be divided into power law creep (including high temperature power law and low temperature power law creep), and power law breakdown creep. These components are individually plotted in Figure 8. Power law breakdown creep becomes active at approximately 375 K and dominates creep mechanisms up to 420 K, reaching a maximum at 400 K. This corresponds to an increasing matrix stress that is also maximum in the vicinity of 400 K.

At higher temperatures, and relatively lower stresses, diffusional creep begins to contribute to the overall creep strain. In this particular case it is a very small contribution compared to the contribution form the dislocation creep mechanisms. As expected, Coble creep is predominant at the lower temperatures, starting around 450 K in Figure 9; and Nabarro-Herring creep is predominant at the higher temperatures, and dominates at a temperature greater than 685 K (Figure 9).

As shown above, the model appears to yield reasonable predictions of the various deformation mechanisms, which dominate during the different temperatures and stresses during the temperature excursions.
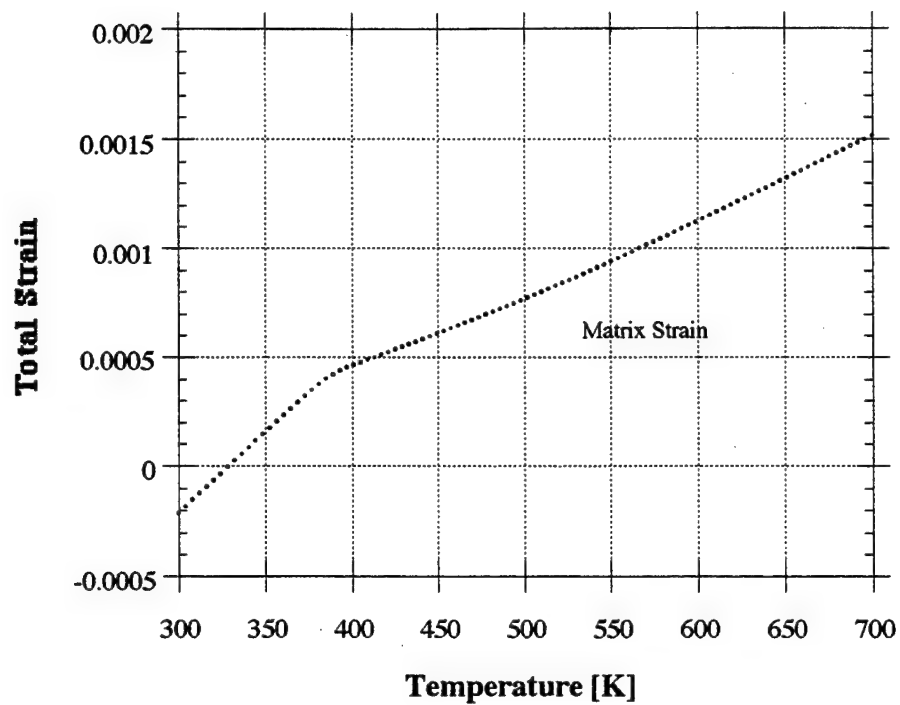
Figure (4) Total cummulative matrix strain during temperature excursion from 300 to 700 K.
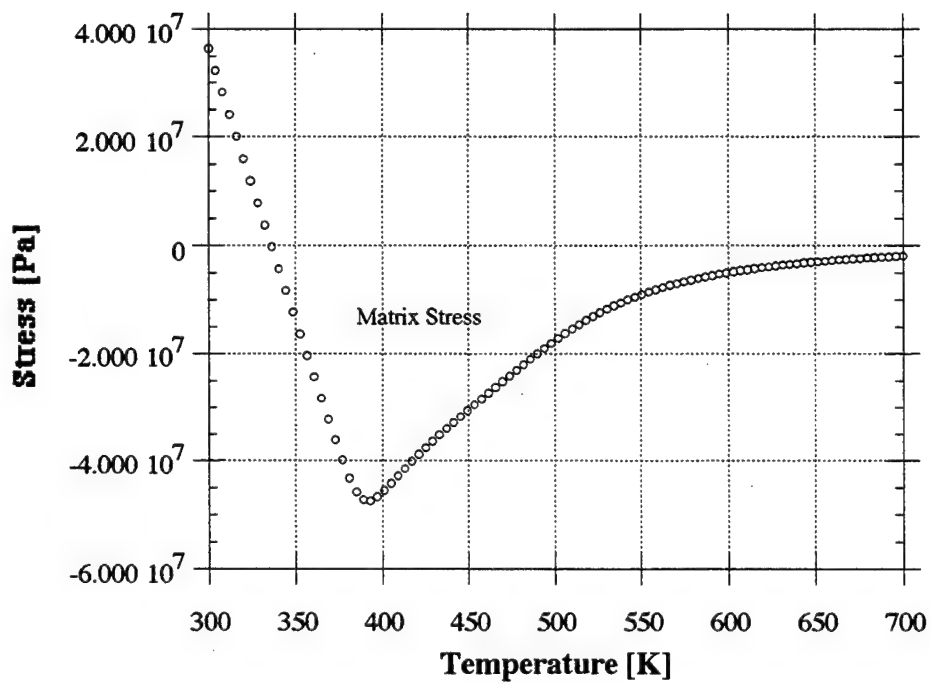
Figure (5) Matrix stress during temperature excursion from 300 to 700 K.

47
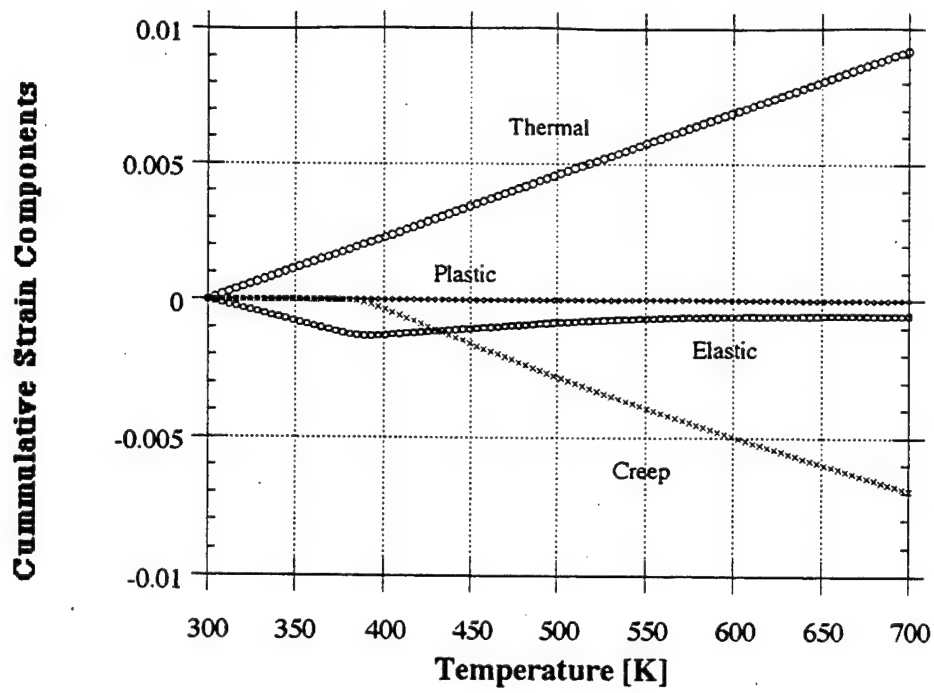
Figure (6)   Cummulative Thermal, Elastic, Plastic, and Creep strains
during the temperature excursion from 300 to 700 K.
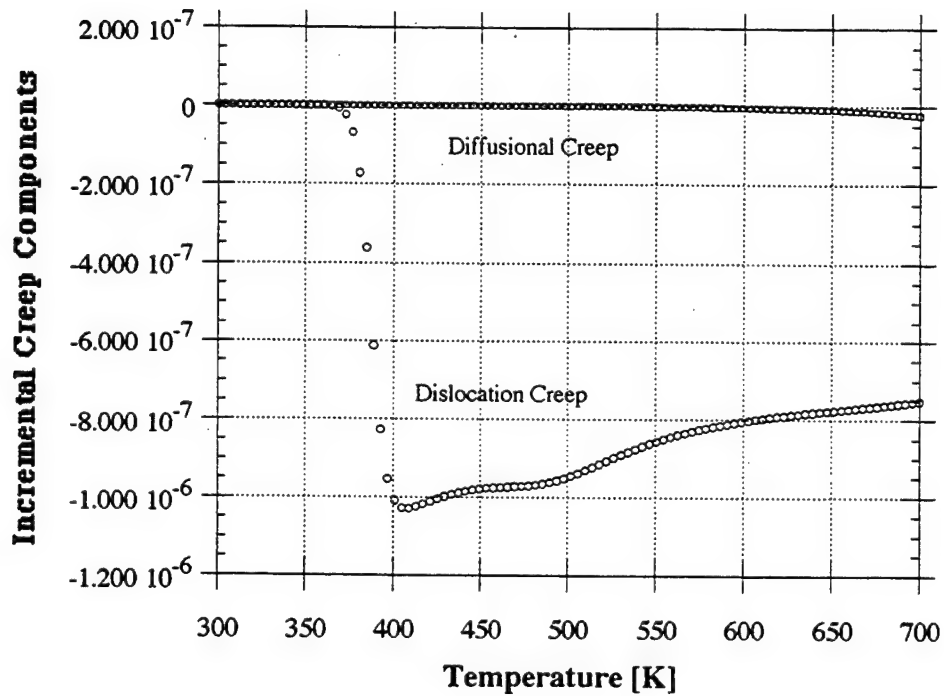
Figure (7)   Dislocational and Diffusional Creep strains during the temperature
excursion from 300 to 700 K.

48
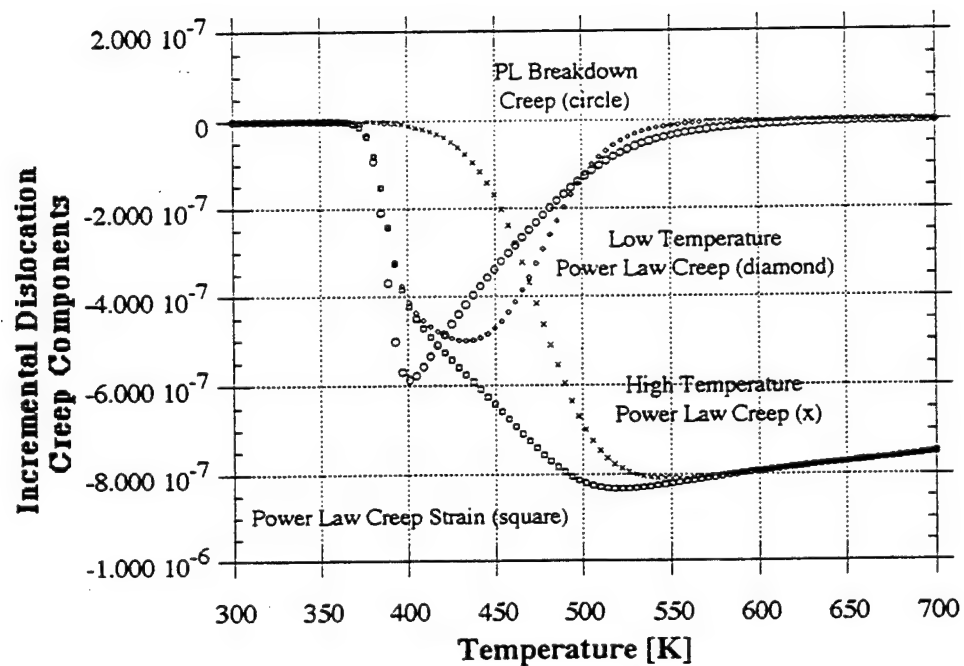
Figure (8)   Total Power Law, which includes high and low Temperature power law creep, and power law breakdown strains during the temperature excursion from 300 to 700 K.

49
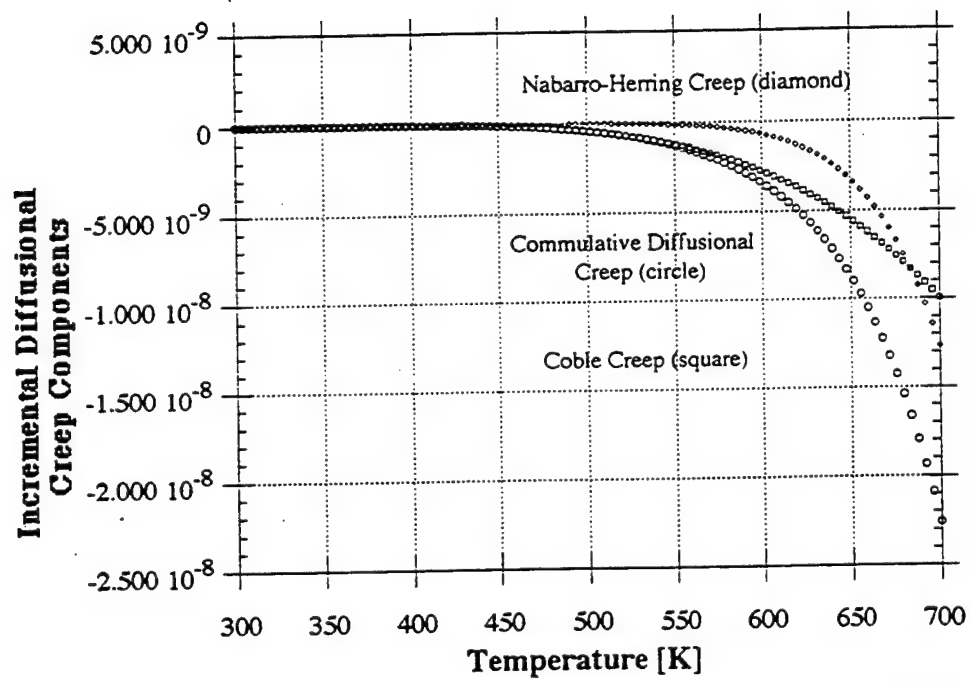
Figure (9)   Total Diffusional Creep which includes the incremental Coble
and Nabarro-Herring Creep strains during temperature excursion
from 300 to 700 K.

D. ISOTHERMAL CREEP WITH CONSTANT APPLIED STRESS

The application of the model to isothermal creep conditions at a temperature of 673 K and under a constant applied load of 50 MPa is discussed for a 40 volume percent continuous SiC fiber reinforced 1100-Al matrix composite with a grain size of 10 μm.

It is to be noted that the applied composite stress of 50 MPa is large enough to cause some plastic deformation of the matrix prior to creep. Figures 10 through 15 represent the various conditions of stresses and strains as the composite commences creeping isothermally with an initial residual compressive matrix stress of 2.4023 MPa and an initial residual strain of -5.0001e-04 (the initial residual matrix stress and residual matrix strain are the results form cooling of the composite from the fabrication temperature to ambient temperature). The behavior is shown only for the first 300 seconds of creep, since rapid changes in stress and strain occur during this initial period under the assumes conditions (50 MPa at 673 K).

Figure 10 shows the cumulative creep strain curve as a function of creep time. Clearly only a primary stage is observed up to 300 seconds. Correspondingly, the matrix stress in Figure 11 is seen to decrease, indicating that the matrix is undergoing stress relaxation, resulting in the progressive transference of the applied stress to the fiber. Interestingly, the matrix stress decreases very rapidly after a few seconds after the starting value and then decreases more slowly. This is because the high initial matrix stress drives the rapid matrix creep, causing accelerated matrix stress relaxation. Figure 12 shows plots of the cumulative matrix elastic and creep strains as a function of creep time. It is

clear that the elastic strain shows a behavior to that of the matrix stress. While the elastic strain drops due to continued stress relaxation, the creep strain increases as expected. Further, there is no plastic strain induced, the matrix stress decreases continuously. Since temperature is a constant, no thermal is induced either.

The individual creep contributions are depicted in Figures 13 through 15. Figure 13 shows that dislocation creep is the predominant deformation mechanism during the early part of the creep. Later (after about 40 seconds), The matrix stress is significantly lower than the starting value, diffusional creep becomes the predominant deformation mechanism, and remains so thereafter. This is because the matrix stress is too low to cause a significant strain rate via dislocation creep.

Figure 14 shows the contribution of the Power Law Breakdown (PLB) and Power Law (PL) mechanism to the overall dislocation creep strain. It is clear that at the relevant applied stress-temperature combination, PL creep is the dominant mechanism. Power law creep may be further subdivided into dislocation pipe diffusion controlled power law creep (Low Temperature Power Law or LTPL) and volume diffusion controlled power law creep (High Temperature Power Law or HTPL). These components are also shown in Figure 14. It is evident that at 673 K, the contribution of HTPL dominates PL creep.

Figure 15 shows the contributions of Coble and Nabarro-Herring components to the total diffusional creep strain at any instant during creep. At the given temperature and stress loads, both mechanisms contribute comparably, with the Coble creep rate being somewhat higher.

All these trends are in quantitative agreement with the trends expected on the basis of steady state deformation maps. Although the initial creep rate is very rapid (i.e., at very low times) appears to be rather too rapid. It is therefore concluded that the model seems to be reasonable mechanistic prediction, it needs to be validated on the basis of extensive experimental work on a simple model system, where the predominant deformation mechanism may be discerned straightforwardly by electron microscopy following creeping to different times.

Thus, it would seem that the model make reasonable prediction for this particular simulation. Actual creep experiments are required to validate model.
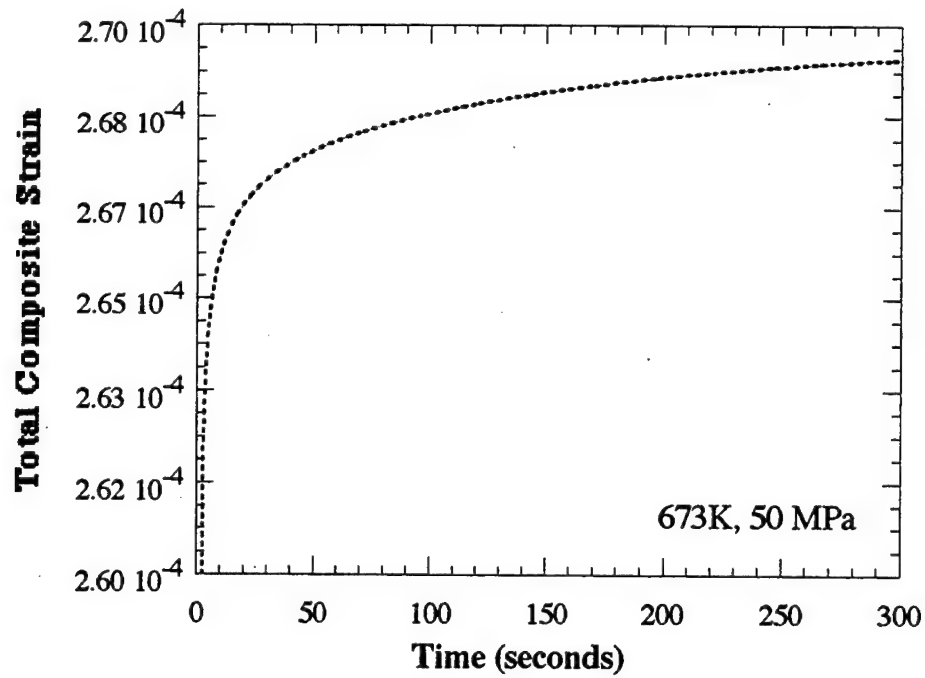
Figure (10)   Total composite stress of a 40 volume percent SiC continuous fiber reinforced 1100-Al matrix composite as a function of creep time at 673 K under an applied composite stress of 50 Mpa.
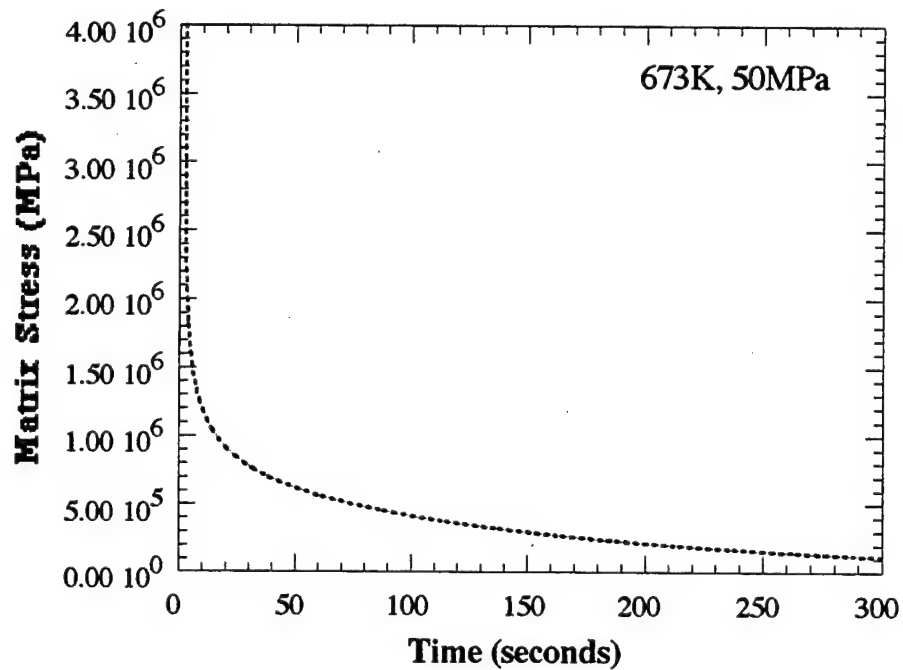
Figure (11)   Variation of matrix stress (σ_m) with time during isothermal creep at 673 K under an applied stress of 50 Mpa.

54
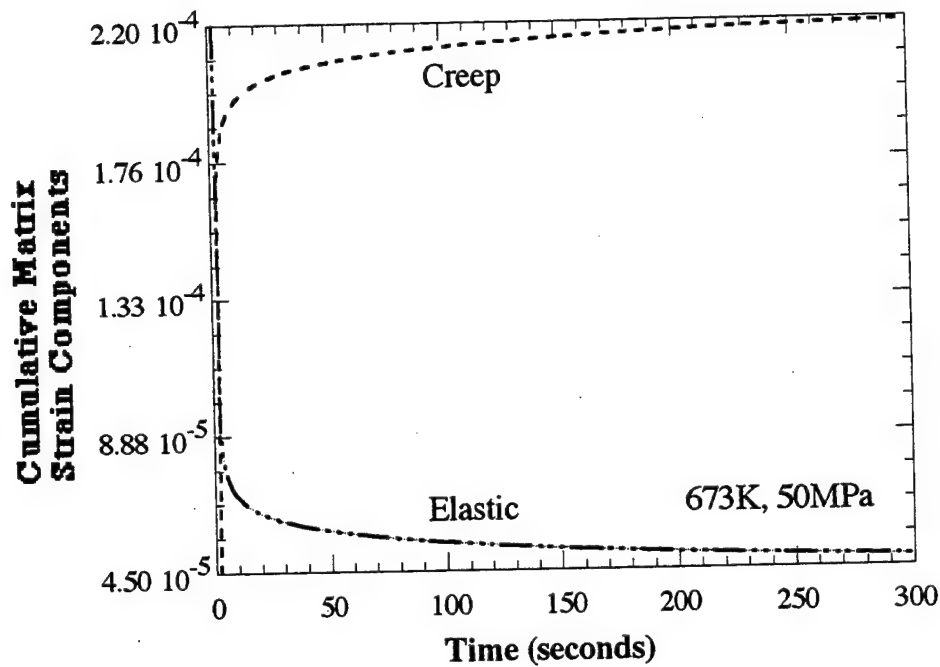
Figure (12)   Variation of total elastic and creep strains as a function of creep time at
               during isothermal creep at 673 K with an applied composite stress of 50
               MPa.
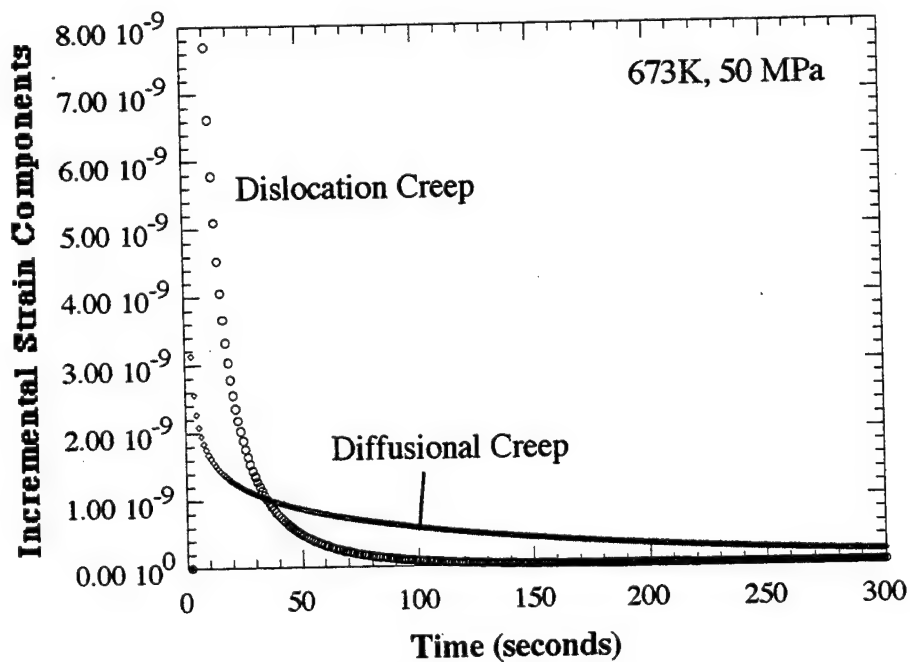
Figure (13)   Instantaneous values of dislocation and diffusional creep strains as
               functions of creep time during isothermal creep at 673 K with an applied
               composite stress of 50 MPa.
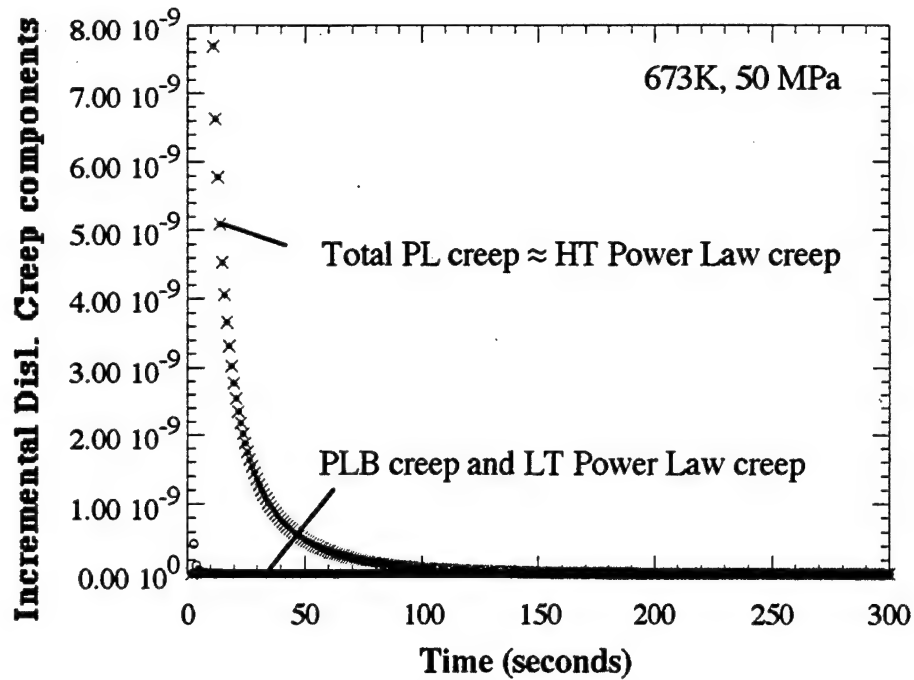
Figure (14)   Instantaneous values of total power law creep strain, comprising of high temperature and low temperature power law creep strains. Also shown is the instantaneous power law breakdown creep strain.
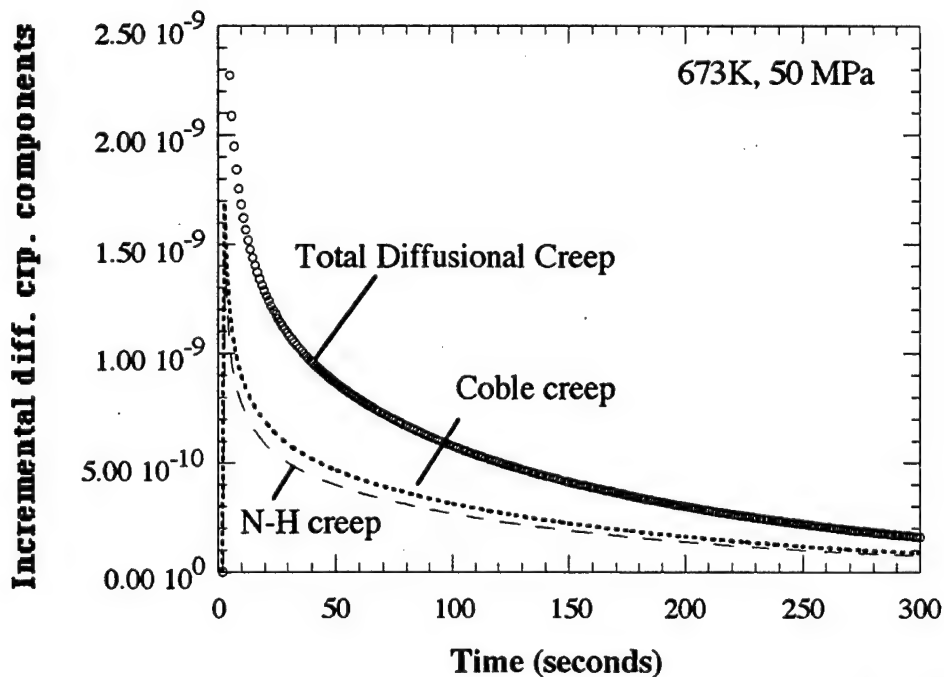
Figure (15)   Instantaneous values of total diffusional creep strain, comprising Coble and Nabarro-Herring creep strains, as functions of creep time during isothermal creep at 673 K with an applied composite stress of 50 MPa.

VI.   SUMMARY

1.   A one-dimensional analytical model for axial deformation of continuous fiber reinforced metal-matrix composites under both thermal cycling and isothermal creep, with or without externally applied stresses, has been developed.   The model assumes that the fiber is thermo-elastic and the matrix is thermo-elastic-plastic-creeping.   The model accounts for the following effects :

a.   Changing dislocation and diffusional matrix creep mechanisms via the use of unified creep laws.   This allows separation of the total matrix creep into dislocation and diffusional creep components.   The dislocation creep strain may be further separated into power-law breakdown and power law creep, including high temperature power law creep (volume diffusion controlled) and low temperature power law creep (dislocation core diffusion controlled), whereas the diffusional creep strain may be split into the Coble and Nabarro-Herring creep components.   This allows the identification of the dominant creep mechanism at any instant during creep/thermal cycling, and is thought to enable the generation of transient deformation mechanism maps in the future.

b.   Time-dependent, diffusional sliding of the interface, following a diffusional flow law with a threshold stress, based on recent experimental studies of single-fiber composites.   The incorporation of such time-dependent interfacial sliding allows simulation of non-isostrain deformation of the

57

fiber and matrix near fiber-ends, where large shear stresses are usually present, and thus is able to explain the frequently observed strain incompatibility between the fiber and matrix, especially during thermal cycling experiments.

c.   Finally, the model is strain-history sensitive, and therefore allows accrual of stresses and strains during a series of thermal and/or load excursions.

2.   Two versions of the model - one excluding interfacial sliding (isostrain model) and one including interfacial sliding (non-isostrain model) have been developed.

3.   Results from two sample calculations (one for constant rate heating without an applied stress and one for isothermal creep in the presence of a constant applied stress), based on the isostrain model are reported, showing the predominance of various creep mechanisms at different times/temperatures.   Because of its ability to calculate the matrix stress state and discern the predominant matrix creep mechanism at any instant during isothermal creep or thermal cycling, it is thought that this model will eventually allow the generation of transient deformation mechanism maps for axial straining of continuous fiber reinforced metal-matrix composites.   The results indicate that the regimes of dominance of the various creep mechanisms are qualitatively reasonable, suggesting that the model is phenomenologically correct.

58

4.   It is recommended that experiments on a simple model system be conducted to

validate the model in the near future.

APPENDIX A. CONVERSION OF SHEAR STRAIN RATE-SHEAR STRESS EQUATIONS TO NORMAL STRAIN RATE-NORMAL STRESS FORMS

A.1 DIFFUSIONAL CREEP

From Frost and Ashby [Ref. 23], we have for the shear strain rate by diffusional creep:

$$\dot{\gamma}_{diff} = \frac{42\sigma_s \Omega}{kTd^2} D_{eff}^{diff} \tag{A.1.1}$$

where $\dot{\gamma}_{diff}$ - shear strain rate for diffusion $D_{eff}^{diff} = D_o e^{-Q/kT}$

σ_s - shear stress [MPa] D_o - frequency factor [$m^2 s^{-1}$]

Ω - atomic volume [m^3] Q - Activation energy for the

k - Boltzman constant [JK^{-1}]   appropriate diffusion path [$kJmol^{-1}$]

d - grain size [m] T - absolute temperature [K]

The von Mises effective stress (σ_m) and strain are related to the matrix shear stress and strain as follows:

$$\sigma_s = \frac{\sigma_m}{\sqrt{3}}$$
$$\dot{\gamma} = \sqrt{3}\dot{\varepsilon}_m \tag{A.1.2}$$

Substitution of Equations (A.1.2) into Equation (A.1.1), and solving for $\dot{\varepsilon}_m^{diff}$ results in Equation (10) found in Section A Chapter IV:

$$\dot{\varepsilon}_m^{diff} = \frac{14\sigma_m \Omega}{kTd^2} D_{eff}^{diff} \tag{10}$$

A.2 DISLOCATION CREEP

From Frost and Ashby [Ref. 23], the shear strain rate by dislocation creep for power-law creep and power-law breakdown is given as:

61

$$\dot{\gamma}_{disl} = A_2' \frac{G_m b D_{eff}}{kT} \left[\sinh\left(\frac{\alpha'}{G_m} \sigma_s \right) \right]^{n'} \qquad (A.2.1)$$

where A_2' is a constant, n' is the stress exponent, and $\dot{\gamma}_{disl}$ is the shear strain rate for

dislocation. For power-law creep, the hyperbolic sine term, $\sinh\left(\dfrac{\alpha'}{G_m} \sigma_s \right)$ approaches

$\dfrac{\alpha'}{G_m} \sigma_s$ in Equation (A.2.1) and becomes:

$$\dot{\gamma}_{PL} = A_2' \frac{G_m b D_{eff}}{kT} \left(\frac{\alpha'}{G_m} \sigma_s \right)^{n'} \qquad (A.2.2)$$

Substituting Equations (A.1.2) in Equation (A.2.2), results in:

$$\dot{\gamma}_{PL} = A_2' \frac{G_m b D_{eff}}{kT} \left(\frac{\alpha'}{G_m} \frac{\sigma_m}{\sqrt{3}} \right)^{n'} \qquad (A.2.3)$$

This is equivalent to the shear stress rate-equation for power-law:

$$\dot{\gamma}_{PL} = A_2 \frac{G_m b D_{eff}}{kT} \left(\frac{\sigma_m}{G_m} \right)^{n} \qquad (A.2.4)$$

Correlating like terms in Equation (A.2.3) and Equation (A.2.4) gives the following:

$$A_2' \alpha'^{n'} = A_2 \qquad (A.2.5)$$

$$n' = n \qquad (A.2.6)$$

Equation (A.2.4) is equivalently written in terms of tensile stress and strain rate and
becomes:

$$\dot{\varepsilon} = \frac{A_2}{\sqrt{3}^{n+1}} \frac{G_m b D_{eff}}{kT} \left(\frac{\sigma_m}{G_m} \right)^{n} \qquad (A.2.7)$$

where the equivalent constant A, for tensile stress and strain rate is represented as:

$$A_2 = \left(\sqrt{3}\right)^{n+1} A \qquad \text{(A.2.8)}$$

$$D_{eff} = D_L + \frac{10}{b^2} a_p \left(\frac{\sigma_s}{G_m}\right)^2 D_p \qquad \text{(A.2.9)}$$

Substituting Equations (A.1.2), and Equations (A.2.7) through (A.2.9) into Equation (A.2.1), and solving for $\dot{\varepsilon}_m^{disl}$ results in Equation (13) found in Section A Chapter IV:

$$\dot{\varepsilon}_m^{disl} = \left(\frac{\sqrt{3}}{\alpha'}\right)^{n1} \frac{AG_m b}{kT} D_{eff} \left[\sinh\left(\frac{\alpha'}{\sqrt{3}} \frac{\sigma_m}{G_m}\right) \right]^{n1} \qquad \text{(13)}$$

where

$$D_{eff}^{disl} = \left[D_L + \frac{10}{3}\left(\frac{a_p}{b^2}\right)\left(\frac{\sigma_m}{G_m}\right)^2 D_p \right]$$

(14)

63

APPENDIX B. MATLAB™ COMPUTER CODE FOR ISOSTRAIN UNIFIED CREEP LAW

% PROGRAM FOR CONT FIBER MMCS WITH RIGID INTERFACE (ISOSTRAIN) AND UNIFIED
% LAW CREEP CAPABLE OF HANDLING A NON-ZERO APPLIED STRESS

%% LAST REVISION DATE : 15 JANUARY 1997

```
clear all
format short e     % Sets floating point format with 5 digits.

M=10000;    .    % M=input('Enter the number of steps, M: ')
PD=100;           % MAKE STEP SIZE (M) LARGER IF DIVISION BY ZERO ERROR OCCURS !!!

                               % DIMENSIONALIZE ARRAY VARIABLES

                               time=zeros(1,M+4);
                               temp=zeros(1,M+4);
                               sigma_m=zeros(1,M+4);
                               sigma_y=zeros(1,M+4);
                               sigma_y1=zeros(1,M+4);
                               d_sigma_m=zeros(1,M+4);
                               d_thstress=zeros(1,M+4);
                               Deff=zeros(1,M+4);
                               Dl=zeros(1,M+4);
                               apDp=zeros(1,M+4);
                               Em=zeros(1,M+4);
                               Gm=zeros(1,M+4);
                               K1=zeros(1,M+4);
                               c=zeros(1,M+4);
                               creep_strain=zeros(1,M+4);
                               total_str=zeros(1,M+4);
                               total_elastic_str=zeros(1,M+4);
                               total_plastic_str=zeros(1,M+4);
                               total_creep_str=zeros(1,M+4);
                               total_thermal_str=zeros(1,M+4);
                               test1=zeros(1,M+4);
                               test2=zeros(1,M+4);
                               num=zeros(1,M+4);
                               den=zeros(1,M+4);
                               invrwh=zeros(1,M+4);
                               rwh=zeros(1,M+4);

                               diff_crp_str=zeros(1,M+4);
                                       NH_crp_str=zeros(1,M+4);
                                       A_NH=zeros(1,M+4);
                                       Coble_crp_str=zeros(1,M+4);
                                       A_Coble=zeros(1,M+4);
                               disl_crp_str=zeros(1,M+4);
                                       PLB_crp_str=zeros(1,M+4);
                                       PL_crp_str=zeros(1,M+4);
                                       LT_PL_crp_str=zeros(1,M+4);
```

65

```
                                    HT_PL_crp_str=zeros(1,M+4);
                                    A_Disl_vol=zeros(1,M+4);
                                    A_Disl_pipe=zeros(1,M+4);
                                    L=zeros(1,M+4);
                            total_disl_crp_str=zeros(1,M+4);
                            total_diff_crp_str=zeros(1,M+4);
```

%%%%%%%%%% ENTER INITIAL AND FINAL CONDITIONS   %%%%%%%%%%%

rate	= -1/60;	% rate=input('Enter Cooling (-) / Heating (+) rate, rate [K/sec]:')
temp_init	= 700;	% temp_init=input('Enter the initial temperature, temp_init [K]:')
temp_final	= 300;	% temp_final=input('Enter the final temperature, temp_final [K]:')
sigma_m_init	= -1.9059e6;	% sigma_m_init=input('Enter the initial matrix stress state,
		% sigma_m_init [Pa]:')
		% sigma_m_init has to be smaller than sigmay1 for isothermal creep
total_str_init	= 1.5156e-3;	% total_str_init=input('Enter the initial total strain, total_str:')
appl_stress	= 0.00e6;	% appl_stress=input('Enter the applied stress, appl_stress [Pa]:')

%%%%%%% INPUT MATERIAL PROPERTIES FOR CALCULATIONS %%%%%%%%%%%%%

T_melt	= 933;	% T_melt=('Enter the matrix Melting Temp., T_melt (K):')
alpha_m	= 23e-6;	% alpha_m=('Enter the matrix CTE, alpha_m [1/K]:')
alpha_f	= 4e-6;	% alpha_f=('Enter the fiber CTE, alpha_f [1/K]:')
Ef	= 450e9;	% Ef=input('Enter Youngs Modulus for the fiber, Ef [Mpa]:')
Vf	= 0.4;	% Vf=input('Enter the volume fraction of the fiber, Vf [0.XX]:')
Emo	= 65e9;	% Emo=input('Enter Matrix Youngs Modulus at 300K, Emo [Mpa]:')
Gmo	= 25e9;	% Gmo=input('Enter Matrix Shear modulus at 300K, Gmo [Mpa]:')
T_Depend	= -0.5;	% T_Depend=input('Enter Temp Dependence of Modulus,
		% (Tm/Go)(dG/dT), T_Depend:')
K1o	= 5e9;	% K1o=input('Enter work hardening constant, K1o [Mpa]:')
n	= 1.0;	% n=input('Enter the work hardening exponent, n:')
Dlo	= 1.7e-4;	% input('Enter the frequency factor for diffusivity), Do [m^2/s]:')
Ql	= 142000;	% input('Enter the Activation Energy for diffusion, Q [J/mole]:')
delDgbo	= 5e-14;	% delDgbo=nput('Enter the Grain Boundary pre-exponential, delta *
		% Dgbo [m^3/s]:')
Qgb	= 84000;	% Qgb=input('Enter the Grain Boundary Activation Energy, Q
		% [J/mole]:')
apDpo	= 7e-25;	% apDp=nput('Enter the Pipe pre-exponential, ap * Dpo [m^4/s]:')
Qp	= 82000;	% Qp=input('Enter the Pipe pre-exponentialActivation Energy, Q
		% [J/mole]:')
b	= 2.86e-10;	% b=input('Enter the Burgers vector, b [m]:')
Omega	= 1.66e-29;	% Omega=input('Enter the Atomic Volume, Omega [m^3]:')
A	= 3.4e6;	% A= input('Dorn Constant [str rate =
		% A*((sigma_m/G)^z)*Deff*G*b/(k*T)], L:')
z	= 4.4;	% z=input('Enter stress exponent for creep equation, z :')
alpha_prime	= 1000;	% alpha_prime=input('alpha_prime, the value of sigma/G for P-L
		% Breakdown, Frost+Ashby:')
d	= 25e-6;	% d=input('Enter the matrix grain size, d [m]:')
R	= 8.314;	% Universal Gas constant [J/mole-K]
K	= 1.38e-23;	% Boltzman constant [J/K]
alpha=alpha_prime/sqrt(3);		% alpha is in tension, alpha_prime in shear (Frost+Ashby)

%%%%% PROPERTIES OF 1100 AL

```
            PP=43.625;
            QQ=-0.009;
            RR=-6.75255e-5;
            MM=35.2082;
            NN=0.0377365;
```

%%%%%%% THIS SECTION CALCULATES THE MATRIX STRESS AFTER APPLYING AN
%%%%%%% EXTERNAL STRESS AT T=temp_init

    % Calculate matrix stress and strain due to appl stress

```
E_m=Emo*(1+((temp_init-300)/T_melt)*T_Depend);     % Find Em at creep temp
G_m=Gmo*(1+((temp_init-300)/T_melt)*T_Depend);     % Find Gm at creep temp
K_1=K1o*(1+((temp_init-300)/T_melt)*T_Depend);     % Find Plastic Modulus at creep
                                                   % temp
E_c=E_m*(1-Vf)+Ef*Vf;                              % Composite modulus at creep
                                                   % temp
```

```
        if appl_stress>0   % associate sign of yield strength with sign of appl_stress
                constant=1;
        else
                constant=-1;
        end
```

%%%%% Yield stress (Pa) of annealed 1100 Al at temp_init

```
if (temp_init <= 625)
        % Power 2 fit for low T region
        sigma_ys=(PP+QQ*temp_init+RR*temp_init^2)*1e6;
else
        % Linear fit for Hi T region
        sigma_ys=(MM-NN*temp_init)*1e6;
end
```

```
            if abs(sigma_m_init)>abs(sigma_ys)
                    sigma_yield=constant*abs(sigma_m_init);
            else
                    sigma_yield=constant*sigma_ys;
            end
```

% SIX VARIOUS APPLICATIONS OF EXTERNAL LOAD TO PRODUCE SIGMA_M_o

```
if sigma_m_init*appl_stress>=0            % initial stress and appl stress have the same sense (sign)
        if abs(sigma_m_init)>=abs(sigma_yield)
                % CASE II : PLASTIC LOADING
                del_sigma_m_app=K_1*appl_stress/(Ef*Vf+K_1*(1-Vf));
                eps=appl_stress/(Ef*Vf+K_1*(1-Vf)) + sigma_m_init/E_m;
                del_strain_app=eps-(sigma_m_init/E_m);   % total strain increment during loading
```

```
            elast_strain=del_sigma_m_app/E_m;          % elastic strain induced in matrix during
                                                       % loading
            plast_strain=del_strain_app-elast_strain;  % plastic strain induced in matrix during
                                                       % loading
    else

        if abs(appl_stress)>=(abs(sigma_yield-sigma_m_init)/E_m)*E_c;
                % CASE I : ELASTO-PLASTIC LOADING
                eps=(appl_stress-((sigma_yield-sigma_m_init)/E_m)*E_c)/(Ef*Vf+K_1*...
                    (1-Vf))+sigma_yield/E_m;
                del_sigma_m_app=(sigma_yield-sigma_m_init)+K_1*(eps-sigma_yield/E_m);
                del_strain_app=eps-(sigma_m_init/E_m);
                elast_strain=del_sigma_m_app/E_m;          % elastic strain induced in matrix
                                                           % during loading
                plast_strain=del_strain_app-elast_strain;  % plastic strain induced in matrix
                                                           % during loading
        else
                % CASE VI : ELASTIC LOADING
                del_sigma_m_app=E_m*appl_stress/E_c;
                eps=(appl_stress/E_c)+(sigma_m_init/E_m);
                del_strain_app=eps-(sigma_m_init/E_m);
                elast_strain=del_sigma_m_app/E_m;          % elastic strain induced in matrix
                                                           % during loading
                plast_strain=0;                            % plastic strain induced in matrix
                                                           % during loading


        end
    end
else      % initial stress and appl stress have opposite signs
        if abs(appl_stress)>=(abs(sigma_yield-sigma_m_init)/E_m)*E_c
                % CASE III : ELASTIC UNLOADING + ELASTIC-PLASTIC LOADING
                eps=(appl_stress-((sigma_yield-sigma_m_init)/E_m)*E_c)/(Ef*Vf+K_1*...
                    (1-Vf))+sigma_yield/E_m;
                del_sigma_m_app=(sigma_yield-sigma_m_init)+K_1*(eps-sigma_yield/E_m);
                del_strain_app=eps-(sigma_m_init/E_m);
                elast_strain=del_sigma_m_app/E_m;          % elastic strain induced in matrix
                                                           % during loading
                plast_strain=del_strain_app-elast_strain;  % plastic strain induced in matrix
                                                           % during loading
        else

            if abs(appl_stress)<=(abs(sigma_m_init))*E_c/E_m
                    % CASE V : ELASTIC UNLOADING ONLY
                    del_sigma_m_app=appl_stress*E_m/E_c;
                    eps=(appl_stress/E_c)+(sigma_m_init/E_m);
                    del_strain_app=eps-(sigma_m_init/E_m);
                    elast_strain=del_sigma_m_app/E_m;          % elastic strain induced in matrix
                                                               % during loading
                    plast_strain=0;                            % plastic strain induced in matrix
                                                               % during loading
            else
                    % CASE IV : EASTIC UNLOADING + ELASTIC LOADING
                    del_sigma_m_app=appl_stress*E_m/E_c;
                    eps=(appl_stress/E_c)+(sigma_m_init/E_m);
```

68

```
                    del_strain_app=eps-(sigma_m_init/E_m);
                    elast_strain=del_sigma_m_app/E_m;        % elastic strain induced in matrix
                                                             % during loading
                    plast_strain=0;                % plast_strain induced in matrix during loading
              end
        end
end


sigma_m_total=sigma_m_init+del_sigma_m_app;    % matrix stress = initial residual stress + applied
                                               % increment
strain_total=total_str_init+del_strain_app;    % matrix strain = starting strain + strain due to appl
                                               % stress
```

%% END OF THE SIX CASES OF APPLIED LOADS

%%%%% The following input stmts are to generalize the prgm for both th cycling and isothermal creep

```
if temp_init==temp_final
        time_init=2;                           % input('Enter the start time, time_init [s]:   ');
        time_final=input('Enter the finish time, time_final [s]:   ');
        time_interval=time_final-time_init;
else
        time_interval=(temp_final-temp_init)/rate;
        time_init=0;
end

        % Set up initial array values

        time(2)=0;                        % time prior to appln of ext stress
        time(3)=1;                        % time corresponding to appln of external stress
        time(4)=time_init;                % time at start of creep or thermal cycling
        temp(2)=temp_init;                % temp at time(2)
        temp(3)=temp(2);                  % temp at time(3)
        temp(4)=temp(3);                  % start temperature for thermal cycling

        total_str(2)=total_str_init;      % initial strain before applying external stress,ie., at time(2)
        total_str(3)=strain_total;        % matrix strain after applying ext stress
        total_str(4)=total_str(3);        % matrix strain just prior to start of creep or thermal cycling

        total_elastic_str(4)=elast_strain;  % elastic strain just after applying external stress
        total_plastic_str(4)=plast_strain;  % plastic strain just after applying external stress

        sigma_m(2)=sigma_m_init;          % matrix stress prior to appln of external stress.
        sigma_m(3)=sigma_m_total;         % matrix stress after applying ext stress
        sigma_m(4)=sigma_m(3);            % matrix stress just prior to start of creep or thermal cycling
```

%%%%%%%%%% START OF CALCULATIONS %%%%%%%%%%

% set time and temp steps

```
timeStep=time_interval/M;              % Calculation of time step.
tempStep=timeStep*rate;                % Calculation of temperature steps.
```

69

```matlab
d_alpha=alpha_m-alpha_f;              % Difference between matrix and Fiber CTE

%%%%%%%%%%%%% BEGIN  ITERATIONS %%%%%%%%%%%%%%%%%%%%%%

for i=5:M+4              % Set counter from 5 to the # of steps plus 4 (M+4)

        temp(i)=temp(i-1)+tempStep;       % New temperature at ith step
        time(i)=time(i-1)+timeStep;       % New time at ith step

        Em(i)=Emo*(1+((temp(i)-300)/T_melt)*T_Depend); % Find Temperature Dependent Em
        Gm(i)=Gmo*(1+((temp(i)-300)/T_melt)*T_Depend); % Find Temperature Dependent Gm
        K1(i)=K1o*(1+((temp(i)-300)/T_melt)*T_Depend);  % Find Temperature Dependent Plastic
                                                        % Modulus

        Dl(i)    = Dlo*exp(-Ql/(R*temp(i)));           % Lattice diffusivity
        apDp(i)  = apDpo*exp(-Qp/(R*temp(i)));         % Pipe diffusivity * area fraction of disln pipe
        Deff(i)  = Dl(i)+(10/3)*apDp(i)*(1/b^2)*(abs(sigma_m(i-1))/Gm(i))^2;
                                                        % Effective Diffusivity for Disl creep
        delDgb(i) = delDgbo*exp(-Qgb/(R*temp(i)));    % Grain Boundary diffusivity*Grain Bdy width

        % Yield stress (Pa) of annealed 1100 Al (T<=625K from Metals Handbook, T>625K assumed)

        if (temp(i) <= 625)
                    % Power 2 fit for low T region
                sigma_y1(i)=(PP+QQ*temp(i)+RR*temp(i)^2)*1e6;
        else
                    % Linear fit for Hi T region
                sigma_y1(i)=(MM-NN*temp(i))*1e6;
        end

        %%%%%%%%%%% Calculate Various Creep Constants %%%%%%%%%%%%

        L(i)=A*((Gm(i)*b)/(K*temp(i)))/(alpha^z); % Pre - Sinh coeff for tension in Frost+Ashby's eqn

                % Nabarro-Herring creep rate = A_NH*sigmam
        A_NH(i)=14*Omega*Dl(i)/(K*temp(i)*d^2);

                % Coble creep rate = A_Coble*sigmam
        A_Coble(i)=14*Omega*(3.14/d)*delDgb(i)/(K*temp(i)*d^2);
                % const for lattice diff contribution in Garofalo's sinh law
        A_Disl_vol(i)=L(i)*Dl(i);
                % const for pipe diff contr. in Sinh law
        A_Disl_pipe(i)=L(i)*(10/3)*apDp(i)*(1/b^2)*(abs(sigma_m(i-1))/Gm(i))^2;

        % CALCULATE UPDATED YIELD STRENGTH

        if (sigma_m(i-1) < 0)                      % for compressive matrix stress
                if (abs(sigma_m(4)) > abs(sigma_y1(5)))
                        sigma_y(i)=-sigma_y1(i)-(abs(sigma_m(2))-abs(sigma_y1(3)));
                else
                        sigma_y(i)=-sigma_y1(i);
                end
                        c(i)=-1;
```

70

```
else              % for tensile matrix stress
        if (abs(sigma_m(4)) > abs(sigma_y1(5)))
                sigma_y(i)=sigma_y1(i)+(abs(sigma_m(2))-abs(sigma_y1(3)));
        else
                sigma_y(i)=sigma_y1(i);
        end
                c(i)=1;
end

%%%%%%%%%%%% FIND rwh  AND  invrwh  %%%%%%%%%%%%%

test1(i)=abs(sigma_m(i-1))-abs(sigma_y(i));
test2(i)=abs(sigma_m(i-2))-abs(sigma_y(i));
DUMMY2(i)=sigma_m(i-1);

if (test1(i) <= 0)
        invrwh(i)=0;
        DUMMY(i) = 5;
else
        if (test2(i) <= 0)
                rwh(i)=K1(i)*n*((abs(sigma_m(i-1)-sigma_y(i)))/K1(i))^((n-1)/n);
                %if (rwh(i)<=1e5)              % when (sigma_m(i-1)-
                % sigma_y(i)) is too large, rwh becomes too small
                %                   invrwh(i)=0;
                % therefore, make inrwh=0 rather than letting it go to infinity
                %else
                        if (sigma_m(i-1)< 0)
                                invrwh(i)=-1/rwh(i);
                        else
                                invrwh(i)= 1/rwh(i);
                        end
                %end

                DUMMY(i) = 10;

        else
                if ((sigma_m(i-1)==sigma_m(i-2)) | (abs(sigma_m(i-1)) < abs(sigma_m(i-2))))
                        invrwh(i)=0;
                        DUMMY(i)=20;
                else
                        rwh(i)=K1(i)*n*((abs(sigma_m(i-1)-sigma_m(i-2)))/K1(i))^((n-1)/n);
                        %if (rwh(i)<=1e5)
                        % when (sigma_m(i-1)-sigma_m(i-2)) is too large, rwh becomes too
                        % small
                        %          invrwh(i)=0;
                        % therefore, make inrwh=0 rather than letting it go to infinity
                                %else
                                        if (sigma_m(i-1)< 0)
                                                invrwh(i)=-1/rwh(i);
                                        else
                                                invrwh(i)= 1/rwh(i);
                                        end
                                %end
                                        71
```

```matlab
                    DUMMY(i)=30;
            end
        end
    end

%%%%%%%%%%%  Find Differential Thermal & Matrix Creep Strains   %%%%%%%%%%%%

    del_th_strain=d_alpha*tempStep;

        NH_crp_str(i)=c(i)*A_NH(i)*abs(sigma_m(i-1))*timeStep;
        Coble_crp_str(i)=c(i)*A_Coble(i)*abs(sigma_m(i-1))*timeStep;

    diff_crp_str(i)=NH_crp_str(i)+Coble_crp_str(i);

%% The following eqns for disln creep are based on Frost+Ashby's Sinh Law

disl_crp_str(i)=c(i)*(A_Disl_vol(i)+A_Disl_pipe(i))*((sinh(alpha*abs(sigma_m(i-1)/Gm(i))))^z) *...
        timeStep;

PL_crp_str(i)=c(i)*(A_Disl_vol(i)+A_Disl_pipe(i))*((alpha*abs(sigma_m(i-1)/Gm(i)))^z)*timeStep;
        LT_PL_crp_str(i)=c(i)*A_Disl_pipe(i)*((alpha*abs(sigma_m(i-1)/Gm(i)))^z)*timeStep;
        HT_PL_crp_str(i)=c(i)*A_Disl_vol(i)*((alpha*abs(sigma_m(i-1)/Gm(i)))^z)*timeStep;
        PLB_crp_str(i)=disl_crp_str(i)-PL_crp_str(i);

    creep_strain(i)=diff_crp_str(i)+disl_crp_str(i);

%%%%%%%%%%%  Find Stress Increments  %%%%%%%%%%%%

    num(i)=del_th_strain+creep_strain(i);
    den(i)=(1/Em(i))+(1-Vf)/(Ef*Vf)+invrwh(i);
    d_sigma_m(i)=-num(i)/den(i);

%%%%%%%%%%%  Find Matrix Stress   %%%%%%%%%%%%

    sigma_m(i)=sigma_m(i-1)+d_sigma_m(i);


%%%%%%%%%%%  Find Matrix Plastic, Elastic & Thermal Strains   %%%%%%%%%%%%

    if ( sigma_m(i-1) < 0 )
            if ( d_sigma_m(i) < 0 )
                    plastic_str(i)=-d_sigma_m(i)*invrwh(i);
            else
                    plastic_str(i)=d_sigma_m(i)*invrwh(i);
            end
    else
            plastic_str(i)=d_sigma_m(i)*invrwh(i);
    end
            elastic_str(i)=d_sigma_m(i)*(1/Em(i));
            thermal_str(i)=alpha_m*tempStep;
```

72

%%%%%%%%%% Find Total Matrix Strain %%%%%%%%%%%

```
        d_strain(i)=elastic_str(i)+plastic_str(i)+creep_strain(i)+thermal_str(i);

        total_str(i)=total_str(i-1)+d_strain(i);
        total_elastic_str(i)=total_elastic_str(i-1)+elastic_str(i);
        total_plastic_str(i)=total_plastic_str(i-1)+plastic_str(i);
        total_creep_str(i)=total_creep_str(i-1)+creep_strain(i);
        total_thermal_str(i)=total_thermal_str(i-1)+thermal_str(i);
                total_diff_crp_str(i)=total_diff_crp_str(i-1)+diff_crp_str(i);
                total_disl_crp_str(i)=total_disl_crp_str(i-1)+disl_crp_str(i);

end

%%%%%%%%%%   PRINT TO A FILE AND PLOT OUTPUTS %%%%%%%%%%%%%%%%%%%%%%

if temp_init == temp_final

        %i=4:M+4;        % Start counter from 2 to include instantaneous strain in total_str vs time plot
        i=linspace(4,M+4,PD);

        figure
        plot(time(i),total_str(i),'o')
        title('Total Strain Vs Time')
        xlabel('TIME [seconds]')
        ylabel('TOTAL STRAIN')

        figure
        plot(time(i),sigma_y(i),'o',time(i),sigma_m(i),'*')
        xlabel('TIME [seconds]')
        ylabel('MATRIX STRESS [Pa]')
        title('Matrix Stress = *,   Yield Strength = o')

        figure
        plot(time(i),total_elastic_str(i),'+',time(i),total_creep_str(i),'d')
        xlabel('TIME [seconds]')
        ylabel('CUMUL. MATRIX STRAIN COMPONENTS')
        title('elastic=+, creep=diamond')
        %title('elastic=+, plastic=o, thermal=*, creep=diamond')

figure
plot(time(i),diff_crp_str(i),'+',time(i),disl_crp_str(i),'o')
xlabel('TIME [seconds]')
ylabel('INCREMENTAL CREEP STRAINS')
title('Diffusional Creep Strain = +,  Dislocation Creep Strain = o')

figure
plot(time(i),disl_crp_str(i),'o',time(i),LT_PL_crp_str(i),'+',time(i),HT_PL_crp_str(i),'*',time(i),PLB_crp_s
tr(i),'d')
xlabel('TIME [seconds]')
ylabel('IND. DISLOCATION CREEP STRAINS')
title('Total Disl Crp=o, LT Power Law=+, HT Power Law=*, PL Breakdown=diamond')
```

73

```
figure
plot(time(i),diff_crp_str(i),'o',time(i),NH_crp_str(i),'+',time(i),Coble_crp_str(i),'*')
xlabel('TIME [seconds]')
ylabel('IND. DIFFUSIONAL CREEP STRAINS')
title('Total Diff Crp = o,   Nabarro-Herring Creep = +,   Coble Creep = *')

%%%%%% PRINT sigma_m AND total_str FOR i=M+4 IN WINDOW   %%%%%%

figure
 orient tall
plot([],[]),axis('off');
text(0.05,1.00,sprintf('ISOTHERMAL CREEP, ISO-STRAIN, UNIFIED CRP. LAW'));
text(0.05,0.95,sprintf('CREEP TEMP [K] = %6.4f',temp_init));
text(0.05,0.90,sprintf('APPLIED STRESS [Pa]= %6.4e',appl_stress));

text(0.10,0.80,sprintf('MATRIX STRESS [Pa] BEFORE APPL STRESS : %6.4e',sigma_m(2)));
text(0.10,0.75,sprintf('MATRIX STRESS [Pa] AFTER APPL STRESS : %6.4e',sigma_m(4)));

text(0.10,0.65,sprintf('TOTAL MATRIX STRAIN BEFORE APPL STRESS: %6.4e',total_str(2)));
text(0.10,0.60,sprintf('TOTAL MATRIX STRAIN AFTER APPL STRESS: %6.4e',total_str(4)));

text(0.15,0.55,sprintf('ELASTIC STRAIN DUE TO APPLIED STRESS:  %6.4e', elast_strain));
text(0.15,0.50,sprintf('PLASTIC STRAIN DUE TO APPLIED STRESS:  %6.4e', plast_strain));

text(0.10,0.40,sprintf('FINAL MATRIX STRESS [Pa]: %6.4e', sigma_m(M+4)));
text(0.10,0.35,sprintf('TOTAL MATRIX STRAIN:  %6.4e', total_str(M+4)));

text(0.10,0.25,sprintf('ELASTIC STRAIN ACCUM. DURING CREEP:  %6.4e', total_elastic_str(M+4)));
text(0.10,0.20,sprintf('TOTAL ISOTHERMAL CREEP STRAIN:  %6.4e', total_creep_str(M+4)));

text(0.10,0.10,sprintf('TOTAL DISL CREEP STRAIN:  %6.4e', total_disl_crp_str(M+4)));
text(0.10,0.05,sprintf('TOTAL DIFF CREEP STRAIN:  %6.4e', total_diff_crp_str(M+4)));

%%%%% DATA OUPUT FILE IS WRITTEN FOR EACH RUN
%%%%% NAME OF DATA FILE MUST DIFER FOR EACH RUN
%%%%% I.E.,  Heat from 300 to 700 K, name file: u3_2_7.txt
%%%%% I.E.,  Creep run at 673 K with 40 MPa applied load, name file: u673_40.txt, etc.

yy=[temp(i);time(i);sigma_y(i);sigma_m(i);total_str(i);...
   total_thermal_str(i);total_elastic_str(i);total_plastic_str(i);total_creep_str(i);...
   disl_crp_str(i);diff_crp_str(i);PLB_crp_str(i);PL_crp_str(i);...
   LT_PL_crp_str(i);HT_PL_crp_str(i);Coble_crp_str(i);NH_crp_str(i)];
fp=fopen('u7_2_3.txt','w');
rowtext=[' temp    time     sigma_y    sigma_m    tot_str   tot_thstr  tot_elstr  tot_plstr  tot_crstr
disl_str   diff_str   PLB_crpstr PL_crpstr  LT_PLstr   HT_PLstr   Coble_str  NH_str     '];
fprintf(fp, ' temp    time     sigma_y    sigma_m    tot_str   tot_thstr  tot_elstr  tot_plstr  tot_crstr
disl_str   diff_str   PLB_crpstr PL_crpstr  LT_PLstr   HT_PLstr   Coble_str  NH_str
\n',rowtext)
fprintf(fp, '%8.2f %10.2f %12.4e %12.4e %12.4e %12.4e %12.4e %12.4e %12.4e %12.4e %12.4e %12.4e
%12.4e %12.4e %12.4e %12.4e %12.4e\n', yy)

else
```

```
i=linspace(4,M+4,PD);

figure
plot(temp(i),total_str(i),'o')
title('Total Strain Vs Temperature')
xlabel('TEMPERATURE [K]')
ylabel('TOTAL STRAIN')

figure
plot(temp(i),sigma_y(i),'o',temp(i),sigma_m(i),'*')
xlabel('TEMPERATURE [K]')
ylabel('MATRIX STRESS [Pa]')
title('Matrix Stress = *,   Yield Strength = o')

figure
plot(temp(i),total_elastic_str(i),'+',temp(i),total_plastic_str(i),'o',temp(i),total_thermal_str(i),'*',temp(i),tot
al_creep_str(i),'d')
xlabel('TEMPERATURE [K]')
ylabel('CUMUL. MATRIX STRAIN COMPONENTS')
title('elastic=+, plastic=o, thermal=*, creep=diamond')

figure
plot(temp(i),diff_crp_str(i),'+',temp(i),disl_crp_str(i),'o')
xlabel('TEMPERATURE [K]')
ylabel('INDIVIDUAL CREEP STRAINS')
title('Diffusional Creep Strain = +,  Dislocation Creep Strain = o')

figure
plot(temp(i),disl_crp_str(i),'o',temp(i),LT_PL_crp_str(i),'+',temp(i),HT_PL_crp_str(i),'*',temp(i),PLB_crp
_str(i),'d')
xlabel('TEMPERATURE [K]')
ylabel('IND. DISLOCATION CREEP STRAINS')
title('Total Disl Crp=o, LT Power Law=+, HT Power Law=*, PL Breakdown=diamond')

figure
plot(temp(i),diff_crp_str(i),'o',temp(i),NH_crp_str(i),'+',temp(i),Coble_crp_str(i),'*')
xlabel('TEMPERATURE [K]')
ylabel('IND. DIFFUSIONAL CREEP STRAINS')
title('Total Diff Crp = o,  Nabarro-Herring Creep = +,   Coble Creep = *')


%%%%%%%% PRINT sigma_m AND total_str FOR i=M+4 IN WINDOW

figure
orient tall
plot([],[]),axis('off');
text(0.05,1.00,sprintf('THERMAL CYCLING, ISO-STRAIN, UNIFIED CREEP'));
text(0.05,0.95,sprintf('INITIAL TEMP = %6.4f',temp_init));
text(0.05,0.90,sprintf('FINAL TEMP = %6.4f',temp_final));
text(0.10,0.85,sprintf('INITIAL MATRIX STRESS [Pa]: %6.4e',sigma_m_init));
text(0.10,0.80,sprintf('INITIAL TOTAL MATRIX STRAIN: %6.4e',total_str(4)));
text(0.10,0.75,sprintf('INITIAL MATRIX ELASTIC STRAIN: %6.4e',total_elastic_str(4)));
```

75

```
text(0.10,0.70,sprintf('INITIAL MATRIX PLASTIC STRAIN:  %6.4e',total_plastic_str(4)));
text(0.10,0.65,sprintf('INITIAL MATRIX THERMAL STRAIN:  %6.4e',total_thermal_str(4)));
text(0.10,0.60,sprintf('INITIAL MATRIX CREEP STRAIN:  %6.4e',total_creep_str(4)));

text(0.10,0.50,sprintf('FINAL MATRIX STRESS [Pa]:  %6.4e', sigma_m(M+4)));
text(0.10,0.45,sprintf('TOTAL MATRIX STRAIN:  %6.4e', total_str(M+4)));

text(0.10,0.35,sprintf('TOTAL ELASTIC STRAIN:  %6.4e', total_elastic_str(M+4)));
text(0.10,0.30,sprintf('TOTAL PLASTIC STRAIN:  %6.4e', total_plastic_str(M+4)));
text(0.10,0.25,sprintf('TOTAL THERMAL STRAIN:  %6.4e', total_thermal_str(M+4)));
text(0.10,0.20,sprintf('TOTAL CREEP STRAIN:  %6.4e', total_creep_str(M+4)));

text(0.10,0.15,sprintf('TOTAL DISL CREEP STRAIN:  %6.4e', total_disl_crp_str(M+4)));
text(0.10,0.10,sprintf('TOTAL DIFF CREEP STRAIN:  %6.4e', total_diff_crp_str(M+4)));

%%%%% DATA OUPUT FILE IS WRITTEN FOR EACH RUN
%%%%% NAME OF DATA FILE MUST DIFER FOR EACH RUN
%%%%% I.E.,  Heat from 300 to 700 K, name file: u3_2_7.txt
%%%%% I.E.,  Creep run at 673 K with 40 MPa applied load, name file: u673_40.txt, etc.

yy=[temp(i);time(i);sigma_y(i);sigma_m(i);total_str(i);...
    total_thermal_str(i);total_elastic_str(i);total_plastic_str(i);total_creep_str(i);...
    disl_crp_str(i);diff_crp_str(i);PLB_crp_str(i);PL_crp_str(i);...
    LT_PL_crp_str(i);HT_PL_crp_str(i);Coble_crp_str(i);NH_crp_str(i)];
fp=fopen('u7_2_3.txt','w');
rowtext=[' temp    time     sigma_y    sigma_m    tot_str    tot_thstr  tot_elstr  tot_plstr  tot_crstr
disl_str  diff_str   PLB_crpstr PL_crpstr  LT_PLstr   HT_PLstr   Coble_str  NH_str     '];
fprintf(fp, ' temp    time     sigma_y    sigma_m    tot_str    tot_thstr  tot_elstr  tot_plstr  tot_crstr
disl_str  diff_str   PLB_crpstr PL_crpstr  LT_PLstr   HT_PLstr   Coble_str  NH_str
\n',rowtext)
fprintf(fp, '%8.2f %10.2f %12.4e %12.4e %12.4e %12.4e %12.4e %12.4e %12.4e %12.4e %12.4e %12.4e
%12.4e %12.4e %12.4e %12.4e %12.4e\n', yy)

end
```

APPENDIX C. DETERMINATION OF THE INTERFACIAL SHEAR STRESS τ_i

In order to determine τ_i, it is assumed that the matrix undergoes elastic, plastic, and creep deformation. For the sake of mathematical expediency, it is further assumed that the matrix creeps by diffusional and power law creep dislocation creep:

$$\gamma_m = \frac{\tau}{G_m} + \frac{\tau - \tau_m^{ys}}{K''} + A'\tau^{n_2} + A''\tau \qquad (C.1)$$

where $\dfrac{\tau}{G_m}$ is the elastic term, $\dfrac{\tau - \tau_m^{ys}}{K''}$ is the plastic term, γ is the shear strain, τ is the interfacial shear stress, τ_m^{ys} is the shear yield strength of the matrix, $A'\tau^{n_2}$ is the dislocation power-law creep term, n_2 is the power-law exponent, A' and A'' are the dislocation power-law creep and diffusional (Coble and Nabarro-Herring) creep terms, respectively.

Since $\gamma_m = \dfrac{dv}{dr}$, Equation (C.1) can be written as:

$$\frac{dv}{dr} = \tau\left(\frac{1}{G_m} + \frac{1}{K''} + A''\right) - \frac{\tau_m^{ys}}{K''} + A'\tau^n \qquad (C.2)$$

Referring to Figure 2 in Section B Chapter IV, consider the displacement along the z-direction at an arbitrary point $(r = r)$ in the matrix, $w(r = r_f) = u$, and $w(r = D/2) = v$. The force equilibrium at $r = r_f$ and arbitrary point $(r = r)$, provides,

$$\tau = \tau_i\left(\frac{r_f}{r}\right) \qquad (C.3)$$

Substitution of Equation (C.3) into Equation (C.1) becomes:

$$\frac{dv}{dr} = \tau_i \frac{r_f}{r}\left(\frac{1}{G_m} + \frac{1}{K''} + A''\right) + A'\left(\tau_i \frac{r_f}{r}\right)^n - \frac{\tau_m^{ys}}{K''} \qquad (C.4)$$

Integrating from $r = r_f$ to R, compared to which $v = (u+w)$ and v respectively, Equation (C.4) becomes:

$$v - (u+w) = \tau_i\left[\frac{1}{G_m} + \frac{1}{K''} + A''\right]r_f \ln\left(\frac{R}{r_f}\right) + A'\tau_i^n r_f^n\left[\frac{R^{1-n} - r_f^{1-n}}{1-n}\right] - \frac{\tau_m^{ys}}{K''}\left(R - r_f\right) \qquad (C.5)$$

Taking the first derivative of Equation (C.5) with respect to z gives:

$$\frac{dv}{dz} - \left(\frac{du}{dz} + \frac{dw}{dz}\right) = \frac{d\tau_i}{dz}\left[\frac{1}{G_m} + \frac{1}{K''} + A''\right]r_f \ln\left(\frac{R}{r_f}\right) + A'n\tau_i^{n-1}\frac{d\tau_i}{dz}r_f^n\left[\frac{R^{1-n} - r_f^{1-n}}{1-n}\right] - 0 \qquad (C.6)$$

Since $\dfrac{dv}{dz} = \varepsilon_m$, $\dfrac{du}{dz} = \varepsilon_f$, and $w = h\gamma_i \Rightarrow$ *therefore* $\dfrac{dw}{dz} = h\dfrac{d\gamma_i}{dz}$.

This time, taking the first derivative of Equation (18) with respect to z, results in $\Rightarrow$

$\dfrac{d\gamma_i}{dz} = K\dfrac{d\tau_i}{dz}\Delta t$, Equation (C.6) becomes

$$\varepsilon_m - \left(\varepsilon_f + hA\frac{d\tau_i}{dz}\right) = \frac{d\tau_i}{dz}\left[\frac{1}{G_m} + \frac{1}{K''} + A''\right]r_f \ln\left(\frac{R}{r_f}\right) + A'n\tau_i^{n-1}\frac{d\tau_i}{dz}r_f^{n-1}\left[\frac{R^{1-n} - r_f^{1-n}}{1-n}\right]$$

$$(C.7)$$

and when rearranged:

$$(\varepsilon_m - \varepsilon_f) = \frac{d\tau_i}{dz}\left[hA + \left(\frac{1}{G_m} + \frac{1}{K''} + A''\right)r_f \ln\left(\frac{R}{r_f}\right) + nA'r_f^n\left(\frac{R^{1-n} - r_f^{1-n}}{1-n}\right)\tau_i^{n-1}\right]$$

$$(C.8)$$

78

For simplicity, let:

$$A = K\Delta t$$

$$A' = A_{disl}\Delta t$$

$$A'' = A_{diff}\Delta t$$

$$M = hKe^{-Q_i/RT}\Delta t$$

$$N = \left(\frac{1}{G_m} + \frac{1}{K''} + A_{diff}\Delta t\right)r_f \ln\left(\frac{R}{r_f}\right)$$

$$Q = nr_f^n A_{disl}\Delta t\left(\frac{R^{1-n} - r_f^{1-n}}{1-n}\right)$$

$$\dot{A}_{diff} = \frac{42\Omega}{kTd^2}\left(D_L + \frac{\pi\delta}{d}D_{gb}\right)$$

$$A_{disl} = \left(\sqrt{3}\right)^{n+1}AD_{eff}\frac{G_m b}{kT}\left(\frac{1}{G_m}\right)^n$$

Equation (C.9) simply becomes:

$$\varepsilon_m - \varepsilon_f = \frac{d\tau_i}{dz}\left[M + N + Q\tau_i^{n-1}\right] \tag{C.9a}$$

If one assumes, ε_f is function of z, and from the second derivative of the force balance

equation ($\tau_i = -\frac{2}{r_f}\frac{d\sigma_f}{dz}$), Equation (C.9a) becomes:

$$\varepsilon_m - \frac{\sigma_f}{E_f} = -\frac{r_f}{2}\frac{d^2\sigma_f}{dz^2}\left[M + N + Q\tau_i^{n-1}\right] \tag{C.9b}$$

or:

$$\frac{d^2\sigma_f}{dz^2} = H1\left[\frac{\sigma_f}{E_f} - \varepsilon_m\right] \tag{C.9c}$$

where:

$$H1 = \frac{2}{r_f}\left[M + N + Q\tau_i^{n-1}\right]$$

and τ_i^{n-1} is the interfacial shear stress from the previous step (iteration).   Equation (C.9c) is a second order differential equation that has a solution of the following form:

$$\sigma_f = E_f \varepsilon_m + C_1 \cosh(\beta z) + C_2 \sinh(\beta z) \qquad (C.10)$$

where: $\beta = \sqrt{\dfrac{H1}{E_f}}$, and applying the following boundary conditions for Equation (C.10):

$$\sigma_f\left(z = \frac{l_o}{2}\right) = 0 \qquad \text{and} \qquad \frac{d\sigma_f\left(z = \dfrac{l_o - l_c}{2}\right)}{dz} = 0$$

C_1 and C_2 becomes:

$$C_1 = -\frac{E_f \varepsilon_m \cosh\left(\beta \dfrac{l_o - l_c}{2}\right)}{\cosh\left(\beta \dfrac{l_c}{2}\right)}$$

$$C_2 = \frac{E_f \varepsilon_m \sinh\left(\beta \dfrac{l_o - l_c}{2}\right)}{\cosh\left(\beta \dfrac{l_c}{2}\right)}$$

Taking the derivative of Equation (C.10) with respect to z, the equation becomes:

$$\frac{d\sigma_f}{dz} = C_1 \beta \sinh(\beta z) + C_2 \beta \cosh(\beta z) \qquad (C.11)$$

The interfacial shear stress τ_i can now be determined by the substitution of Equation (C.11) in the force balance equation which results in:
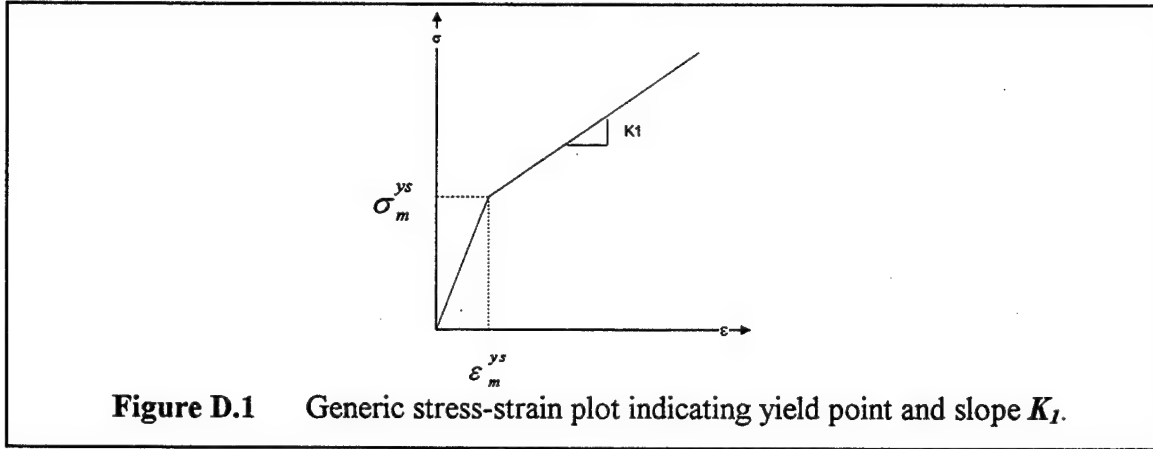
$$\tau_i = -\frac{2}{r_f}\left[C_1 \beta \sinh(\beta z) + C_2 \beta \cosh(\beta z)\right] \qquad (C.12)$$

where C_1, C_2 and β have all been defined earlier.

APPENDIX D. RELATIONSHIP BETWEEN THE LINEAR WORK HARDENING COEFFICIENTS IN SHEAR, K'' AND TENSION, K_1

As determined from Figure D.1, the stress at any point of the plot is:

$$\sigma = E_m \varepsilon_m^{ys} + K_1 \left(\varepsilon_{m-} \varepsilon_m^{ys} \right) \tag{D.1}$$

Figure D.1   Generic stress-strain plot indicating yield point and slope K_1.

Substitution of the von Mises criterion, $\tau = \dfrac{\sigma}{\sqrt{3}}$ and $\gamma = \sqrt{3}\varepsilon$ in Equation D.1,

$$\tau = \frac{E_m}{3} \gamma_m^{ys+} + \frac{K_1}{3} \left(\gamma - \gamma_m^{ys} \right) \tag{D.2}$$

Young's Modulus, E_m is a function of the Shear Modulus,

$$G_m \Rightarrow G_m = \frac{E_m}{2(1+v)} \tag{D.3}$$

where v is Poisson's ratio.   Substitute Equation (D.3) in Equation (D.2)

$$\Rightarrow \quad \tau = \frac{2(1-v)G_m}{3} \gamma_m^{ys} + \frac{K_1}{3} \left(\gamma - \gamma_m^{ys} \right) \text{ and compare to } \Rightarrow \quad \tau = G_m \gamma_m^{ys} + K'' \left(\gamma - \gamma_m^{ys} \right).$$

Assuming mathematical license, $v \cong 0.5$, thus $2(1+v) \cong 3$, then

$$K'' = \frac{K_1}{3} \tag{D.4}$$

APPENDIX E. TEMPERATURE DEPENDENCE OF THRESHOLD STRESS, τ_o

The interfacial shear strain rate obtained from Reference 40 may be represented as:

$$\dot{\gamma} = \frac{4\delta_i D_i \Omega_i}{kTh^2}\left[\tau_i + \tau_o\right] \tag{E.1}$$

where τ_o is given by:

$$\tau_o = 2\pi^3\left(\frac{h}{\lambda}\right)^3 \sigma_R \tag{E.2}$$

and σ_R, the radial (normal) stress is a function of temperature acting on τ_o. The radial stress, σ_R is assumed a linear function of temperature, of the form:

$$\sigma_R = \frac{A}{T} + C \tag{E.3}$$

where A and C are arbitrary constants. Application of the two initial conditions for Equation (E.3), (1) is at the stress free conditions at composite fabrication, and (2) is at room temperature,

$$\sigma_R(T = 800K) = 0 \qquad\qquad \sigma_R(T = 300K) = \sigma_{R_o}$$

where σ_{Ro} is not to exceed the matrix yield strength, the constants A and C are determined to be:

$$A = 480\sigma_{R_o} \qquad\qquad C = -0.60\sigma_{R_o}$$

Substitution of the constants A and B into Equation (E.3), Equation (E.3) becomes:

$$\sigma_R = \frac{480\sigma_{R_o}}{T} - 0.60\sigma_{R_o}$$

The final form of Equation (E.2) for τ_o is:

$$\tau_o = 2\left(\frac{\pi h}{\lambda}\right)^3\left[\frac{480}{T} - 0.60\right]\sigma_{R_o} \tag{E.4}$$

83

LIST OF REFERENCES

1. Cahn, R. W., E. A. Davis, and I. M. Ward, *Microstructural Design of Fiber Composites*, Cambridge University Press (1991), pp. 1-28.

2. Ashbee, K. H. G., *Fundamental Principles of Fiber Reinforced Composites*, (1989), p. xi.

3. Donomoto, T., K. Funatani, N. Muira and N. Miyake, *Ceramic Fiber Reinforced Piston for High Performance Diesel Engines*, (1983), SAE paper 830252.

4. Ebisawa, M., T. Hava, T. Hayashi, and H. Ushio, *Production Process of Metal Matrix Composite (MMC) Engine Block*, (1991), SAE paper 910835.

5. Kelly, A., and W.R. Tyson, *Tensile Properties of Fiber Reinforced Metals--II. Creep of Silver*-Tungsten, J. Mech. Phy. Solids, (1966), **14**, pp. 177-186.

6. De Silva, A. R. T., *Theoretical Analysis of Creep in Fibre Reinforced Composites*, Mech. Phys. Solids, (1963), **16**, pp. 169-186.

7. Doruk, M. and A. S. Yue, *Creep Behavior of Fiber Reinforced Metal Matrix*, Metallurgical Transactions A, (1976), **7A**, 1976, p. 1465.

8. McLean, M., *Creep Deformation of Metal-Matrix Composites*, Composite Science and Technology, (1985), **23**, pp. 37-52.

9. Matsuura, K., M. Chou and N. Matsuda, *Creep Deformation and Fracture of an Aluminum Composite Reinforced with Continuous Alumina Fibers*, Material Transactions, JIM, (1991), **32**, no. 11, pp. 1062-1070.

10. Bullock, E., M. McLean and D. E. Miles, *Creep Behavior of a Ni-Ni$_3$Al-Cr$_3$C$_2$ Eutectic Composite*, Acta Metallurgica, (1977), **25**, pp. 333-344.

11. Goto, S., and M .McLean, *The Role of Interfaces in Creep in Fiber Reinforced Metal Matrix Composites--I. Continuous Fibers*, Acta Metallurgica at Materialia, (1991), **39**, no. 1, pp. 153-164.

12. Dlouhy, A., G. Eggeler, and N. Merk, *A Microstructural Study of Creep in Short Fiber Reinforced Aluminum Alloys*, (1993), **41**, no.11, pp. 3245-3256.

13. Dlouhy, A., G. Eggeler, and N. Merk, *A Micromechanical Model for Creep in Short Fiber Reinforced Aluminum Alloys*, (1995), **42**, no. 2, pp. 535-550.

14. Dragone, T. L. and W. D. Nix, *Steady State and Transient Creep Properties of an Aluminum Alloy Reinforced with Alumina Fibers*, Acta Metallurgica at Materialia, (1992), **40**, no. 10, pp. 2781-2791.

15. Meier, M. and W. Blum, *Modeling High Temperature Creep of Academic and Industrial Materials Using the Composite Model*, Material Science and Engineering, (1993), **A164**, pp. 290-294.

16. Dutta I., S. Mitra and A. D. Wiest, *Residual Stresses in Composites-Measurement, Modeling and Effects on Thermo-Mechanical Behavior*, E. V. Barrera and I. Dutta, eds., TMS-AIME (1993) p. 273.

17. Mitra S., I. Dutta and R. C. Hansen, *Thermal Cycling Studies of a Cross-Plied P100 Graphite Fibre-reinforced 6061 Aluminum Composite Laminate*, Journal of Materials Science, (1991), **26**, p. 6223.

18. Garmong, G., *Elastic-Plastic Analysis of Deformation Induced by Thermal Stress in Eutectic Composites: II. Thermal Expansion*, Metallurgical Transactions A, (1974), **5,** pp. 2191-2197.

19. Gonzalez-Doncel, G. and O. D. Sherby, *Tensile Ductility and Fracture of Superplastic Aluminum-SiC Composites Under Thermal Cycling Conditions*, Metallurgical and Materials Transactions A, (1996), 27A, pp. 2837-2842.

20. Wu M. Y and O. D. Sherby, Scripta Metall. (1984), **18**, p. 773.

21. Wu M. Y., J. Wadsworth and O. D. Sherby, Metall, Trans. (1987), **18A**, p. 451.

22. Flour J. C. and R. Locicero, Scripta Metall. (1987), **21**, p. 1071.

23. Frost H. J. and M. F. Ashby, *Deformation Mechanism Maps: The Plasticity and Creep of Metals and Ceramics*, Pergamon Press, (1982).

24. Jech, R.W. and E. P. Weber, *Cleveland Research Center Final Report*, (1957), Contract No. 55-953-C.

25. Dean, A. V., Journal Institute of Metals, (1966).

26. Ellison, E. G. and B. Harris, Applied Mater. Res., (1966), **5**, p. 33.

27. Ashby, M. F., *A First Report on Deformation Mechanism Maps*, Acta Metallurgica, (1972), **20**, pp. 887-901.

28. Yoda S., N. Kurihara, K. Wakashima and S. Umekawa, *Thermal Cycling-Induced Deformation of Fibrous Composites With Particular Reference to the Tungsten-Copper System*, Metallurgical Transactions A, (1978), **9A**, p. 1229-1236.

29. Miracle, Daniel B., WL/MLLM, WPAFB, OH, (1997), private communication.

30. Rosler, J., G. Bao, and A. G. Evans, *The Effects of Diffusional Relaxation on the Creep Strength of Composites, Acta Metallurgica at Materialia,* **39**, no. 11, pp. 2733-2738.

31. Kim, K. T., and R. M. McMeeking, *Power Law Creep with Interface Slip and Diffusion in a Composite Material,* Mechanics of Materials, (1995), **20**, pp. 153-164.

32. Nimmagata, P. B. R. and P. Sofronis, *Creep Strength of Fiber and Particulate Composite Materials: The Effect of Interface Slip and Diffusion,* (1996), Mechanics of Materials, **23**, pp. 1-19.

33. Weber, C. H., J. Y. Yang, P. A. Lofvander, C. G. Levi and A. G. Evans, *The Creep and Fracture Resistance of γ-TiAl Reinforced with Al_2O_2 Fibers,* Acta Metallurgica at Materialia, (1993), **41**, no. 9, pp. 2681-2690.

34. Schwenker, S. W., and D. Eylon, *Creep Deformation and Damage in Continuous Fiber-Reinforced Ti-6Al-4V Composite,* Metallurgical and Materials Transactions A, (1996), **27A**, pp. 4193-4204.

35. Dragone, T. L., J. J. Schlautmann, and W. D. Nix, *Processing and Creep Characterization of a Model Metal Matrix Composite: Lead Reinforced with Nickel Fibers,* Metallurgical and Materials Transactions A, (1991), **22A**, pp. 1029-1036.

36. Funn, J.V., *Creep Behavior of the Interface Region in Continuous Fiber Reinforced Metal Matrix Composites,* Naval Postgraduate School Thesis, (1997), pp. 1-96.

37. Garmong, G., *Elastic-Plastic Analysis of Deformation Induced by Thermal Stress in Eutectic Composites: I. Theory,* Metallurgical Transactions A, (1974), **5,** pp. 2183-2190.

38. Tyson, W. R., *Discussion of "Elastic-Plastic Analysis of Deformation Induced by Thermal Stress in Eutectic Composites",* Metallurgical and Materials Transactions A, (1975), **6A,** pp. 1674-1677.

39. Dutta, I., *Creep and Thermal Cycling of Continuous Fiber Reinforced Metal-Matrix Composites,* Key Engineering Materials, (1995), **104-107**, pp. 673-690.

40. Dries, G. A., and S. S. Tompkins, NASA TP #2612, NASA-Langley Research Center, Hampton, Virginia (1986).

41. Garafalo, F., *An Empirical Relation Defining the Stress Dependence of Minimum Creep Rate in Metals*, Transactions of the Metallurgical Society of AIME, (1963), **227**, pp. 351-356.

42. CRC Handbook of Chemistry and Physics, 77th Edition, 1996-1997, (1996), CRC Press.

43. Metals Handbook, Properties and Selection: Nonferrous Alloys and Special Purpose Materials, Tenth Edition, (1990), ASM International.

INITIAL DISTRIBUTION LIST

1. Defense Technical Information Center.. 2
   8725 John J. Kingman Rd., STE 0944
   FT. Belvoir, Virginia 22060-6218

2. Dudley Knox Library.. 2
   Naval Postgraduate School
   411 Dyer Rd.
   Monterey, California 93943-5100

3. Naval Engineering, Code 34... 1
   Naval Postgraduate School
   Monterey, California 93943-5100

4. Department Chairman, Code ME/Mc... 1
   Department of Mechanical Engineering
   Naval Postgraduate School
   Monterey, California 93943-5000

5. Professor Indranath Dutta, Code ME/Du.. 1
   Department of Mechanical Engineering
   Naval Postgraduate School
   Monterey, California 93943-5000

6. Dr. Bruce A. MacDonald... 1
   Program Director
   Metal, Ceramics, and Electronic Materials
   National Science Foundation
   Materials Research Division
   4201 Wilson Blvd. Rm. 1065
   Arlington, VA 22230

7. Dr. Daniel B. Miracle.. 1
   Metallic Composites Research Group Leader
   AF Wright Laboratory
   Materials Directorate
   WL/MLLM Bldg 655
   2230 Tenth St. Suite 1
   WPAFB, OH 45433